

## ELECTRONIC SUPPLEMENTARY INFORMATION

### Extending Human Perception of Electromagnetic Radiation to the UV Region through Biologically Inspired Fuzzy Logic Photochromic Systems

Pier Luigi Gentili,\*<sup>a</sup> Amanda Rightler,<sup>a,b</sup> B. Mark Heron,<sup>c</sup> Christopher D. Gabbott<sup>c</sup>

<sup>a</sup>Department of Chemistry, Biology and Biotechnology, University of Perugia,  
Via Elce di sotto 8, 06123 Perugia, Italy

<sup>b</sup>Department of Chemistry and Biochemistry, University of Tulsa, Tulsa, Oklahoma, USA

<sup>c</sup>Department of Chemical and Biological Sciences, School of Applied Science,  
University of Huddersfield, Queensgate, Huddersfield, HD1 3DH, UK

#### Contents:

	Page N°
Experimental Section – General comments	3
General reaction scheme for the preparation of the naphthopyrans <b>2 – 5</b>	5
Experimental method for the preparation naphthopyran <b>2</b>	5
Figure S1 <sup>1</sup> H NMR spectrum of compound <b>2</b> in CDCl <sub>3</sub>	6
Figure S2 <sup>13</sup> C NMR spectrum of compound <b>2</b> in CDCl <sub>3</sub>	6
Figure S3 Mass Spectral data for compound <b>2</b>	7
Figure S4 UV-vis spectra of <b>2</b> before and after UV activation	10
Experimental method for the preparation naphthopyran <b>3</b>	10
Figure S5 <sup>1</sup> H NMR spectrum of compound <b>3</b> in CDCl <sub>3</sub>	11
Figure S6 <sup>13</sup> C NMR spectrum of compound <b>3</b> in CDCl <sub>3</sub>	11
Figure S7 Mass Spectral data for compound <b>3</b>	12
Figure S8 UV-vis spectra of <b>3</b> before and after UV activation	15
Experimental method for the preparation naphthopyran <b>4</b>	15
Figure S9 <sup>1</sup> H NMR spectrum of compound <b>4</b> in CDCl <sub>3</sub>	16
Figure S10 <sup>13</sup> C NMR spectrum of compound <b>4</b> in CDCl <sub>3</sub>	16
Figure S11 Mass Spectral data for compound <b>4</b>	17
Figure S12 UV-vis spectra of <b>4</b> before and after UV activation	19
Experimental method for the preparation naphthopyran <b>5</b>	20
Figure S13 <sup>1</sup> H NMR spectrum of compound <b>5</b> in CDCl <sub>3</sub>	21
Figure S14 <sup>13</sup> C NMR spectrum of compound <b>5</b> in CDCl <sub>3</sub>	21
Figure S15 Mass Spectral data for compound <b>5</b>	22
Figure S16 UV-vis spectra of <b>5</b> before and after UV activation	25
Experimental determinations of the photochemical quantum yields ( $\Phi_{PC}$ ) at different Irradiation wavelengths in the UV, the bleaching kinetic constants ( $k_A$ ) and the molar Absorption coefficients of the coloured species	26
Figure S17 Spectra recorded for <b>1</b> before UV irradiation (black trace) and at the photostationary state (red trace)	27
Figure S18 Effect of the UV irradiation on the spectrum of <b>2</b>	28

Figure S19 Effect of the UV irradiation on the spectrum of <b>3</b>	28
Figure S20 Effect of the UV irradiation on the spectrum of <b>4</b>	29
Figure S21: Effect of UV irradiation on the spectrum of <b>5</b>	29
Quantum mechanical simulations of the absorption spectra of the uncoloured forms of <b>1 – 5</b>	30
Figure S22 Electronic absorption spectrum of <b>1</b> (red trace) compared with the simulated oscillator strengths of the optically active transitions	31
Table S1 The principal optically active transitions of <b>1</b> , simulated by DFT 6-31G including the contribution of acetonitrile	31
Figure S23 Molecular orbitals involved in the most optically active electronic transitions of <b>1</b>	32
Figure S24: Electronic absorption spectrum of <b>2</b> (red trace) compared with the simulated oscillator strengths of the optically active transitions	34
Table S2 The principal optically active transitions of <b>2</b> , simulated by DFT 6-31G including the contribution of acetonitrile	34
Figure S25 Molecular orbitals involved in the most optically active electronic transitions of <b>2</b>	35
Figure S26 Electronic absorption spectrum of <b>3</b> (red trace) compared with the simulated oscillator strengths of the optically active transitions	37
Table S3 The principal optically active transitions of <b>3</b> , simulated by DFT 6-31G including the contribution of acetonitrile	37
Figure S27 Molecular orbitals involved in the most optically active electronic transitions of <b>3</b>	38
Figure S28 Electronic absorption spectrum of <b>4</b> (red trace) compared with the simulated oscillator strengths of the optically active transitions	40
Table S4 The principal optically active transitions of <b>4</b> , simulated by DFT 6-31G including the contribution of acetonitrile	40
Figure S29 Molecular orbitals involved in the most optically active electronic transitions of <b>4</b>	41
Figure S30 Electronic absorption spectrum of <b>5</b> (red trace) compared with the simulated oscillator strengths of the optically active transitions	43
Table S5 The principal optically active transitions of <b>5</b> , simulated by DFT 6-31G including the contribution of acetonitrile	43
Figure S31: Molecular orbitals involved in the most optically active electronic transitions of <b>5</b>	44
Reflectance properties of paper impregnated with the best quaternary mixture after irradiation by UVA, UVB and UVC	45
Figure S32: Reflectance spectra paper impregnated with best dye composition after irradiation with UVA (A), UVB (B) and UVC (C)	45

## Experimental Section – General comments

Unless otherwise stated, reagents were used as supplied by major chemical suppliers.  $^1\text{H}$  (400 MHz) and  $^{13}\text{C}$  (100 MHz) NMR spectra (Bruker Avance) were recorded in  $\text{CDCl}_3$ . FT-IR spectra were recorded on a Nicolet 380 FT-IR spectrophotometer equipped with a diamond ATR attachment (neat sample). Flash column chromatography was performed on chromatography silica gel (Sigma-Aldrich, 40-63 micron particle size distribution). All compounds were homogeneous by TLC using a range of eluent systems of differing polarity [Merck TLC aluminium sheets either silica gel 60 F254 (cat. No 105554) or neutral aluminium oxide 60 F254 (cat. No 105550)]. High resolution mass spectra were recorded under electrospray ionization using a linear ion trap mass spectrometer [Thermo Scientific LTQ Orbitrap XL Fourier transform mass spectrometer, EPRSC National Mass Spectrometry Service, Swansea]. UV-visible characterization spectra were recorded in spectroscopic grade toluene solutions of the samples (10 mm path length quartz cuvette, PTFE capped, concentration ranges *ca.*  $3 \times 10^{-4} - 10^{-5}$  mol dm $^{-3}$ ) using an Agilent Technologies Cary 60 spectrophotometer equipped with a temperature controlled (20 °C) stirred cell. Irradiation of the stirred sample solutions was accomplished with a Spectroline 8 Watt TLC inspection lamp at 365 nm. 1,1-Bis(4-methoxyphenyl)prop-2-yn-1-ol,<sup>S1</sup> 1,1-diphenylprop-2-yn-1-ol,<sup>S2</sup> 3-(2-fluorophenyl)-3-(4-pyrrolidinophenyl)-3*H*-naphtho[2,1-*b*]pyran **5**,<sup>S3</sup> were freshly prepared according to literature procedures. 4-Morpholino-2-naphthol and 1-(4-morpholinophenyl)-1-phenylprop-2-yn-1-ol, were provided by James Robinson Ltd., (Vivimed Laboratories Europe, Huddersfield, UK). 3,4-Dimethyl-1-naphthol was obtained according to the procedures described by Tietze and Eicher<sup>S4</sup> which were derived from those reported by Arnold *et al.*,<sup>S5</sup> and by Cromwell *et al.*<sup>S6,S7</sup> Characterization data ( $^1\text{H}$  and  $^{13}\text{C}$  NMR, IR and UV-vis spectra together with mass spectral data) are reported for all compounds since some of the photochromic molecules employed in this study have only been described with incomplete characterization data in the patent literature.

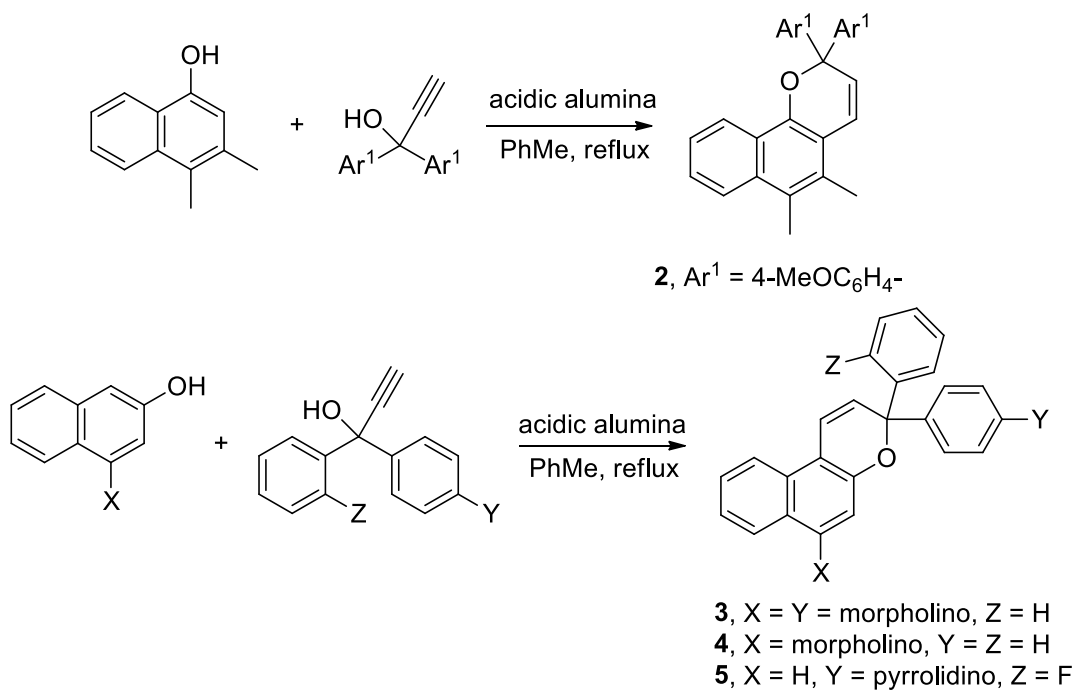
1,3-Dihydro-1,3,3-trimethyl-8'-nitro-spiro[2*H*-indole-2,3'-[3*H*]naphth[2,1-*b*][1,4]oxazine] (1)  
(supplied by Great Lakes Chemical Italia S.r.l.) was used as received after checking its high degree of purity by an HPLC technique.

For the spectrophotometric measurements, acetonitrile (from Fluka, ≥99.8%) was used as solvent. The photochromic species were dissolved in acetonitrile in concentrations ranging from  $10^{-5}$  to  $10^{-3}$  mol dm $^{-3}$ . Pieces of filter white paper (3 cm x 3 cm) purchased from Cordenons (67 g/m $^2$ ) were soaked in a petri dish containing a thin layer of photochromic solution and were maintained within a freezer for at least 30 minutes.

## References

- S1 D. A. Thomas, S. M. Partington, M. B. Hursthouse, T. Gelbrich, *Eur. J. Org. Chem.*, **2003**, 1220.
- S2 V. Maraval, C. Duhayon, Y. Coppel, R. Chauvin, *Eur. J. Org. Chem.*, **2008**, 5144.
- S3 C. D. Gabbutt, B. M. Heron, A. C. Instone, *Heterocycles*, **2003**, *60*, 843.
- S4 Reactions and Synthesis in the organic Chemistry Laboratory, by L. F. Tietze and Th. Eicher, University Science Books (Mill Valley, California) **1989**, pp 115 – 116, p 139, p 256 and pp 273 – 274.
- S5 R. T. Arnold, J. S. Buckley (Jr), J. Richter, *J. Am. Chem. Soc.*, **1947**, *69*, 2322.
- S6 R. D. Campbell, N. H. Cromwell, *J. Am. Chem. Soc.*, **1955**, *77*, 5169.
- S7 V. L. Bell, N. H. Cromwell, *J. Org. Chem.*, **1958**, *23*, 789.

**General reaction scheme for the preparation of the naphthopyrans 2 – 5.**



**Preparation of 2,2-Bis(4-methoxyphenyl)-5,6-dimethyl-2*H*-naphtho[1,2-*b*]pyran: 2**

A stirred solution of 2,3-dimethyl-1-naphthol (1.50 g, 8.71 mmol) and 1,1-bis(4-methoxyphenyl)prop-2-yn-1-ol (2.34 g, 8.71 mmol) in toluene (125 mL) was warmed to 50 °C. Acidic alumina (4.0 g) was added and the mixture was heated under reflux until none of the prop-2-yn-1-ol remained by TLC (ca. 2.5 h). The mixture was cooled to ca. 50 °C and filtered and the alumina was washed with hot toluene (2 × 50 mL). Removal of the toluene from the combined washings and filtrate gave a deep red gum that was eluted from silica with 25% EtOAc in *n*-hexane to afford the naphthopyran **2** 1.95 g, 53% as off-white micro-crystals after crystallization from *n*-hexane / EtOAc, mp = 152 – 154 °C;  $\nu_{\max}$  2967, 2839, 2810, 1604, 1506, 1467, 1298, 1246, 1172, 1110, 1062, 974, 825, 763, 661, 586, 578 cm<sup>-1</sup>;  $\delta_{\text{H}}$  2.43 (3H, s, Me), 2.51 (3H, s, Me), 3.76 (6H, s, OMe), 6.18 (1H, d, *J* = 9.9 Hz, 3-H), 6.82 – 6.85 (4H, m, Ar-H), 6.97 (1H, d, *J* = 9.9 Hz, 4-H), 7.41 – 7.49 (6H, m, Ar-H, 8-H, 9-H), 7.92 (1H, dd, *J* = 8.3, 1.2 Hz, 7-H), 8.38 (1H, dd, *J* = 8.1, 1.3 Hz, 10-H);  $\delta_{\text{C}}$  14.6, 15.8, 55.2, 81.5, 113.4, 115.6, 121.5, 122.5, 123.6, 123.7, 123.8, 124.3, 126.2, 127.9, 128.2, 129.3, 133.4, 137.7, 146.1, 158.8. Found [M+H]<sup>+</sup> = 423.1949, C<sub>29</sub>H<sub>26</sub>O<sub>3</sub> requires [M+H]<sup>+</sup> = 423.1955.

**Figure S1:**  $^1\text{H}$  NMR Spectrum of 2,2-Bis(4-methoxyphenyl)-5,6-dimethyl-2*H*-naphtho[1,2-*b*]pyran (**2**)

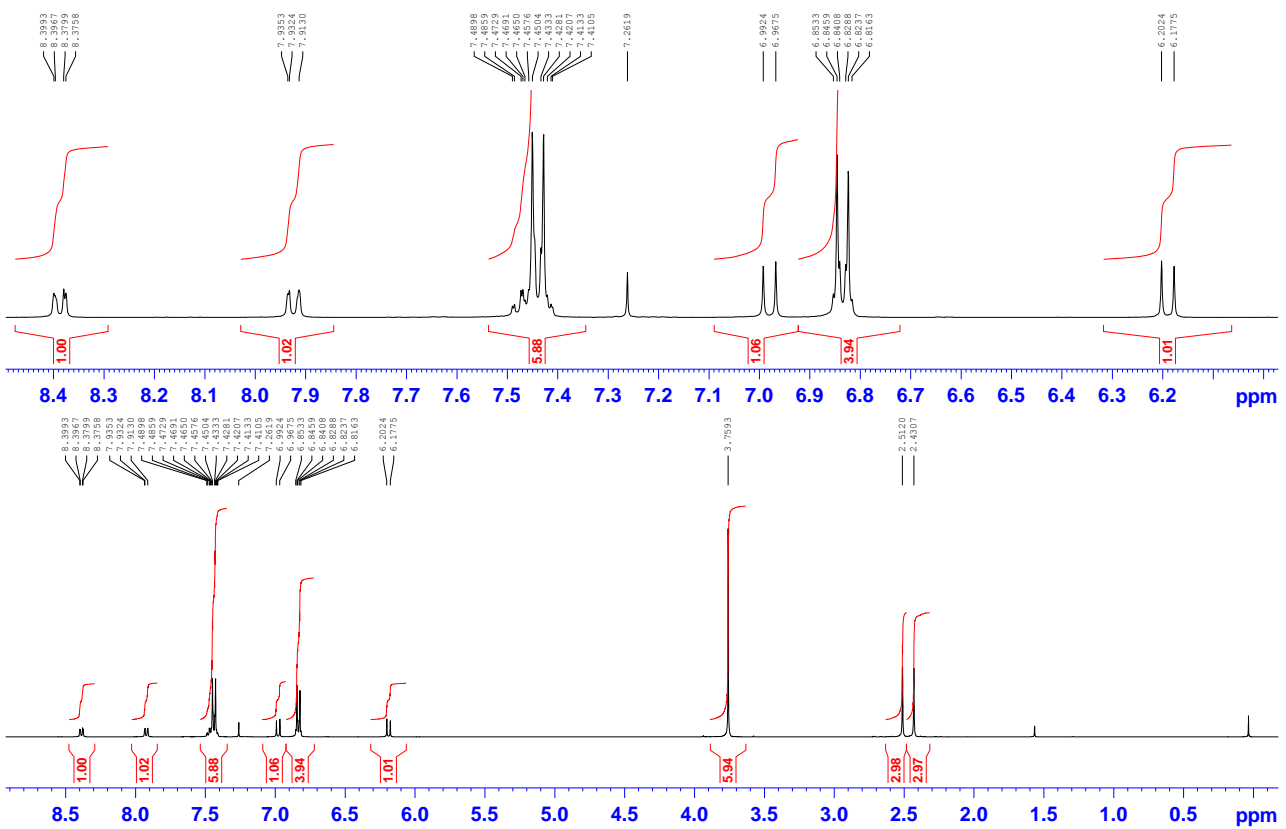


**Figure S2:**  $^{13}\text{C}$  NMR Spectrum of 2,2-Bis(4-methoxyphenyl)-5,6-dimethyl-2*H*-naphtho[1,2-*b*]pyran (**2**)

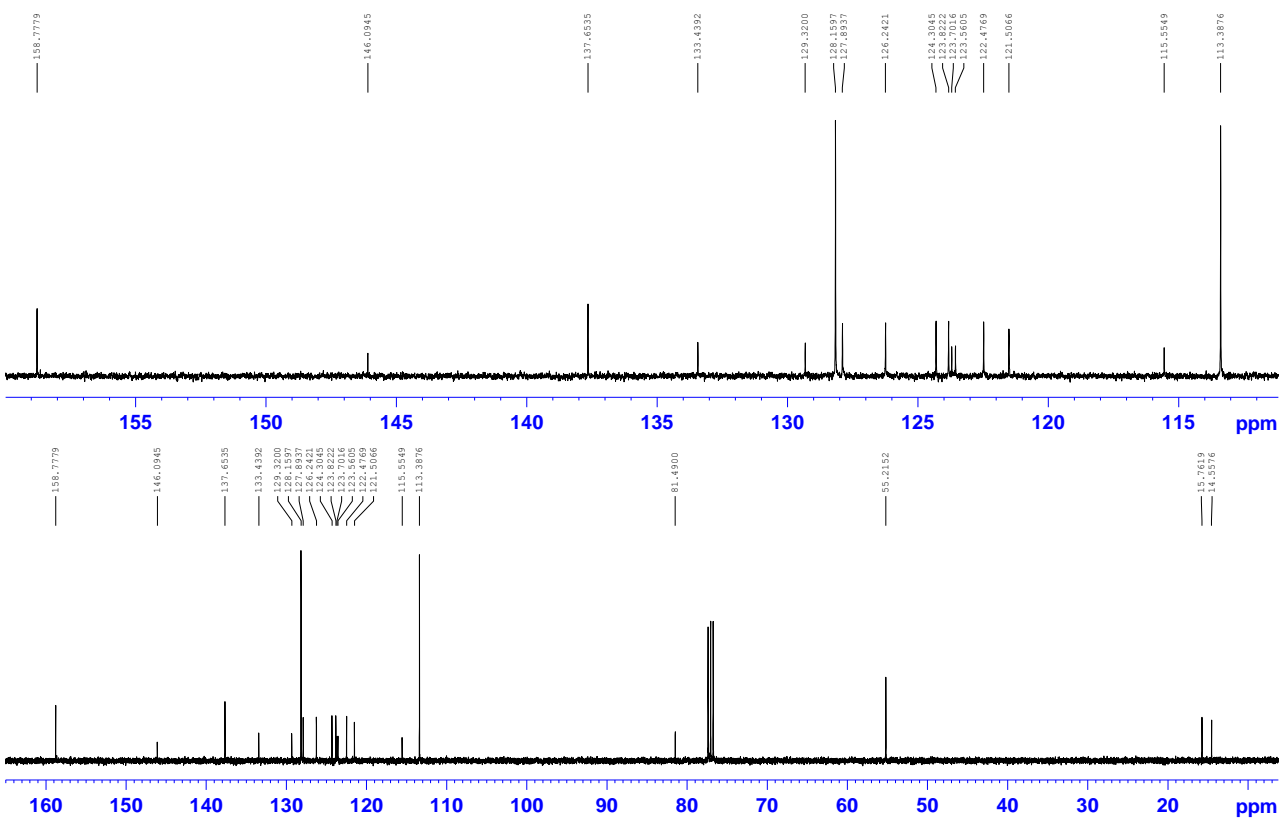
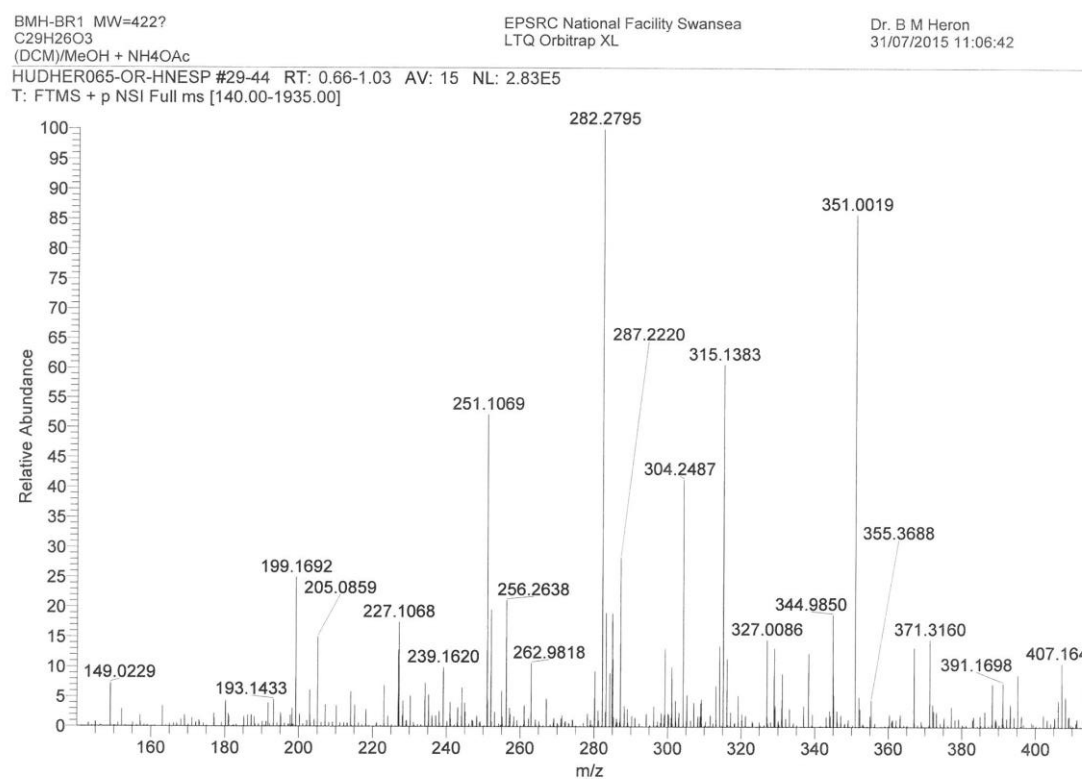
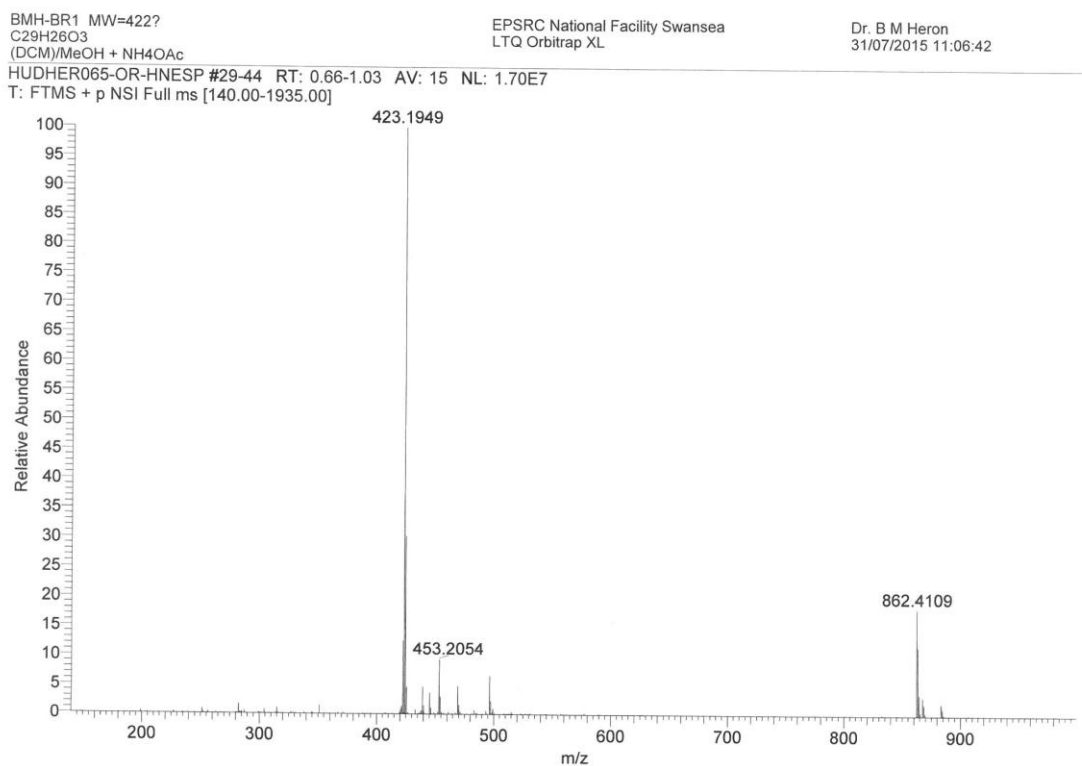


**Figure S3:** Mass Spectral data for 2,2-Bis(4-methoxyphenyl)-5,6-dimethyl-2*H*-naphtho[1,2-*b*]pyran (**2**)

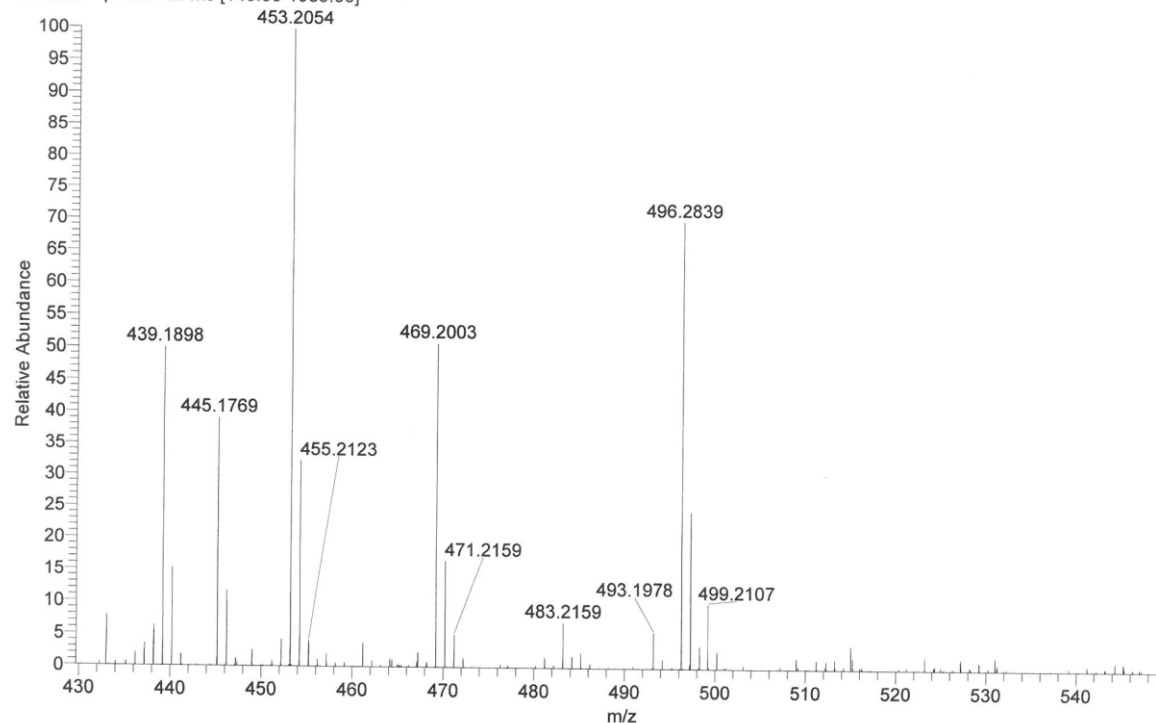


BMH-BR1 MW=422?  
C<sub>29</sub>H<sub>26</sub>O<sub>3</sub>  
(DCM)/MeOH + NH<sub>4</sub>OAc

EPSRC National Facility Swansea  
LTQ Orbitrap XL

Dr. B M Heron  
31/07/2015 11:06:42

HUDHER065-OR-HNESP #29-44 RT: 0.66-1.03 AV: 15 NL: 1.60E6  
T: FTMS + p NSI Full ms [140.00-1935.00]

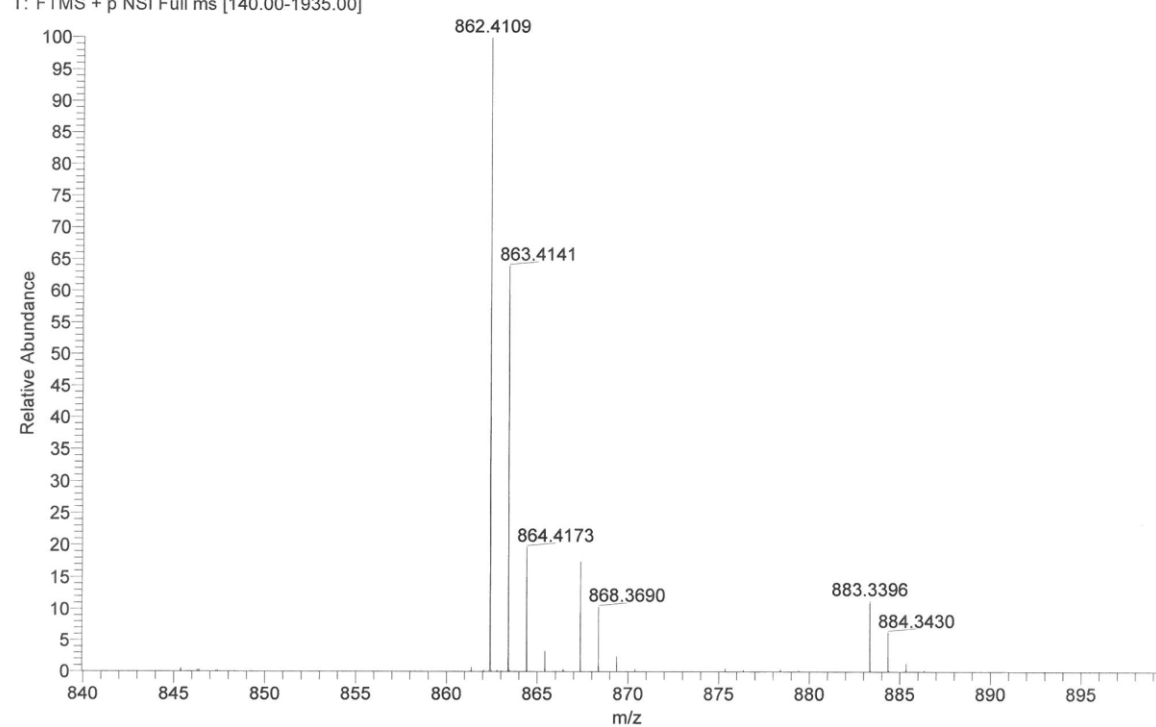


BMH-BR1 MW=422?  
C<sub>29</sub>H<sub>26</sub>O<sub>3</sub>  
(DCM)/MeOH + NH<sub>4</sub>OAc

EPSRC National Facility Swansea  
LTQ Orbitrap XL

Dr. B M Heron  
31/07/2015 11:06:42

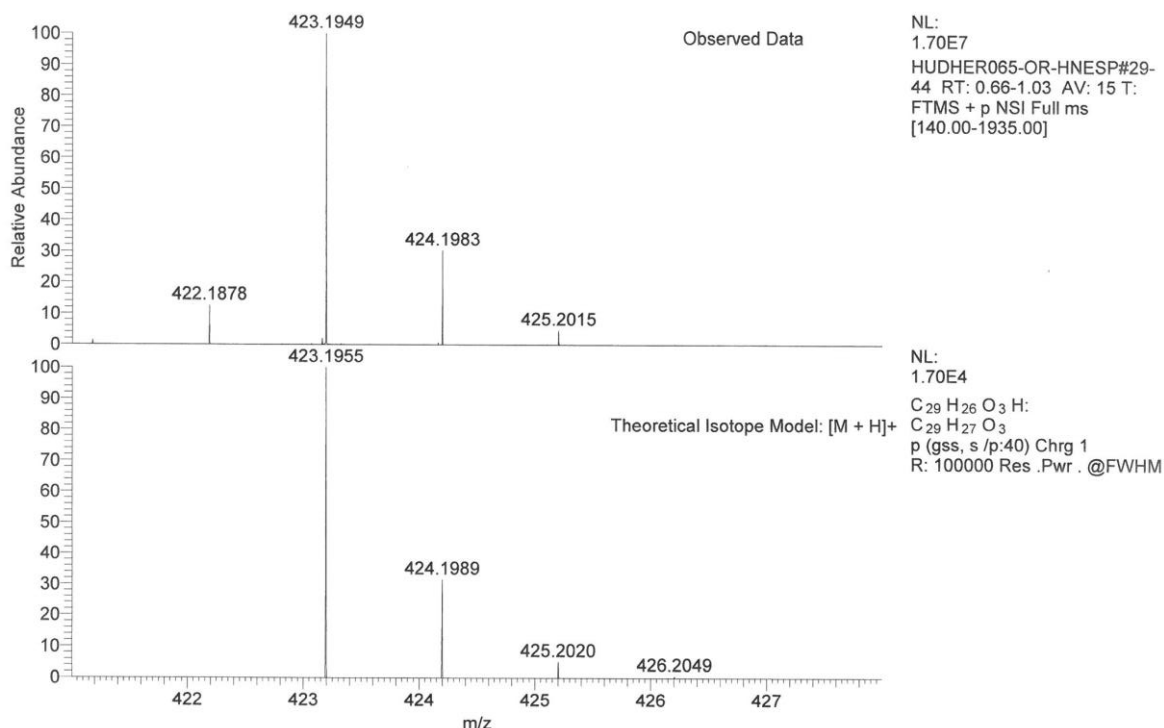
HUDHER065-OR-HNESP #29-44 RT: 0.66-1.03 AV: 15 NL: 3.10E6  
T: FTMS + p NSI Full ms [140.00-1935.00]



BMH-BR1 MW=422?  
C<sub>29</sub>H<sub>26</sub>O<sub>3</sub>  
(DCM)/MeOH + NH<sub>4</sub>OAc

EPSRC National Facility Swansea  
LTQ Orbitrap XL

Dr. B M Heron  
31/07/2015 11:06:42



**Isotope:** Min. ... Max.

14 N 0....10  
16 O 0....10  
12 C 0....60  
1 H 0....80  
23 Na 0....0

Tolerance Window: +- 5.00 ppm

Db/Ring Equiv: -3.. 100

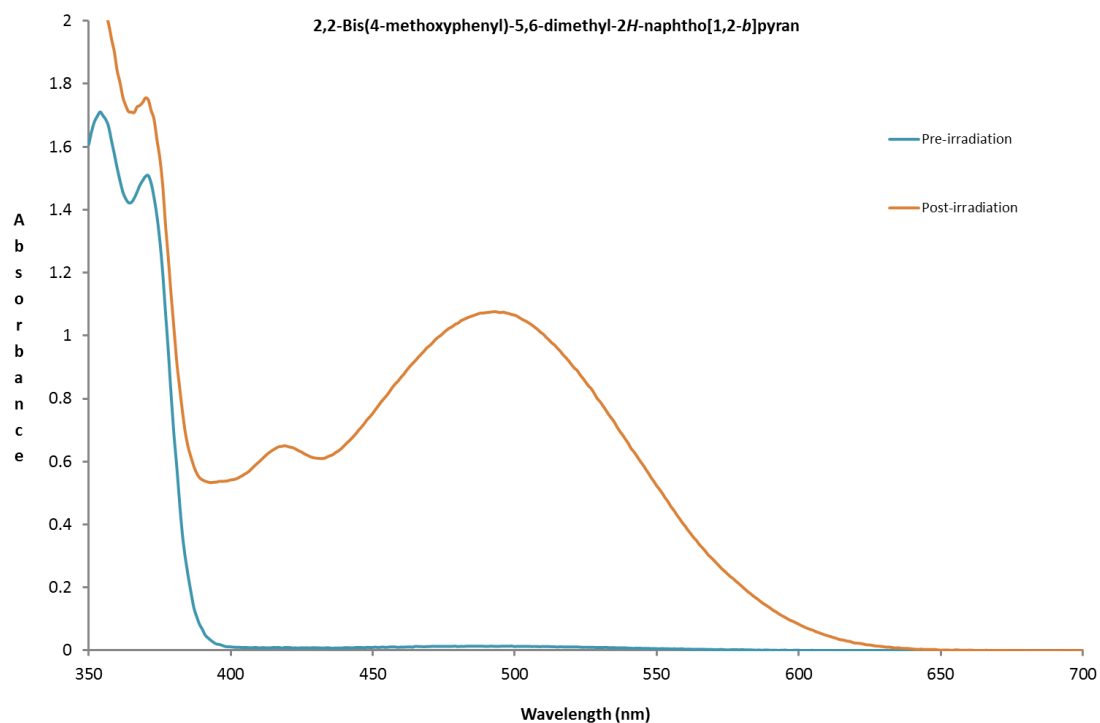
Fits: 100

N-Rule: Do not use

Charge: 1

Mass	Theoretical Mass	Delta [ppm]	RDB	Composition
423.1949	423.1946	0.6	4.5	C <sub>13</sub> H <sub>27</sub> O <sub>8</sub> N <sub>8</sub>
	423.1955	-1.3	16.5	C <sub>29</sub> H <sub>27</sub> O <sub>3</sub>
	423.1941	1.8	17.0	C <sub>27</sub> H <sub>25</sub> O <sub>2</sub> N <sub>3</sub>
	423.1960	-2.5	4.0	C <sub>15</sub> H <sub>29</sub> O <sub>9</sub> N <sub>5</sub>
	423.1928	5.0	17.5	C <sub>25</sub> H <sub>23</sub> O <sub>1</sub> N <sub>6</sub>

**Figure S4:** UV-vis spectra of **2** before and after UV activation



#### Preparation of 6-Morpholino-3-(4-morpholinophenyl)-3-phenyl-3*H*-naphtho[2,1-*b*]pyran: **3**

A stirred solution of 4-morpholino-2-naphthol (1.50 g, 6.5 mmol) and 1-(4-morpholinophenyl)-1-phenylprop-2-yn-1-ol (1.92 g, 6.5 mmol) in toluene (125 mL) was warmed to 50 °C. Acidic alumina (4.0 g) was added and the mixture was heated under reflux until none of the prop-2-yn-1-ol remained by TLC (ca. 1.5 h). The mixture was cooled to ca. 50 °C and filtered and the alumina was washed with hot toluene (2 × 50 mL). Removal of the toluene from the combined washings and filtrate gave a deep red gum that was eluted from silica with 50% EtOAc in *n*-hexane to afford the naphthopyran **3** 2.40 g, 72.0 % as colourless micro-needles after crystallization from EtOAc / *n*-hexane, mp = 187 – 189 °C;  $\nu_{\text{max}}$  2962, 2846, 1613, 1585, 1514, 1262, 1205, 1115, 1019, 902, 844, 764, 746, 704, 689, 517 cm<sup>-1</sup>;  $\delta_{\text{H}}$  3.09 – 3.10 (4H, m, N(CH<sub>2</sub>)<sub>2</sub>), 3.14 (4H, t, *J* = 4.8 Hz, N(CH<sub>2</sub>)<sub>2</sub>), 3.83 (4H, d, *J* = 4.8 Hz, O(CH<sub>2</sub>)<sub>2</sub>), 3.96 (4H, d, *J* = 4.5 Hz, O(CH<sub>2</sub>)<sub>2</sub>), 6.13 (1H, d, *J* = 9.9 Hz, 2-H), 6.83 (1H, s, 5-H), 6.83 – 6.86 (2H, m, Ar-H), 7.23 – 7.39 (7H, m, Ar-H, 1-H), 7.43 – 7.50 (3H, m, Ar-H), 7.94 (1H, d, *J* = 8.4 Hz, 7-H), 8.07 (1H, d, *J* = 8.0 Hz, 10-H);  $\delta_{\text{C}}$  49.0, 53.4, 66.9, 67.3, 82.7, 107.6, 109.9, 114.9, 119.1, 121.9, 123.1, 124.0, 124.4, 125.9, 126.7, 126.9, 127.4, 128.1, 128.2, 131.0, 136.1, 145.4, 150.4, 151.0, 151.3. Found [M+H]<sup>+</sup> = 505.2477, C<sub>33</sub>H<sub>32</sub>N<sub>2</sub>O<sub>3</sub> requires [M+H]<sup>+</sup> = 505.2486.

**Figure S5:**  $^1\text{H}$  NMR spectrum of 6-Morpholino-3-(4-morpholinophenyl)-3-phenyl-3*H*-naphtho[2,1-*b*]pyran (**3**)

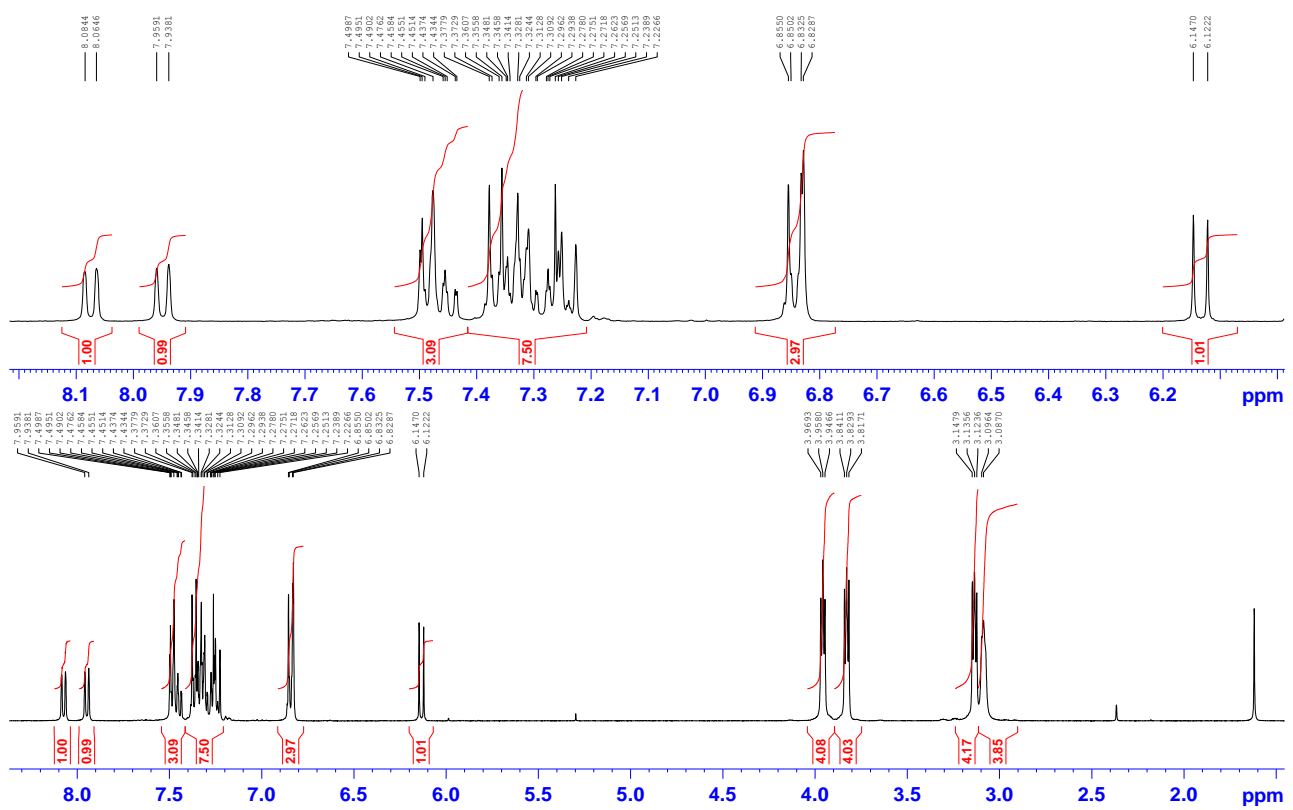


**Figure S6:**  $^{13}\text{C}$  NMR spectrum of 6-Morpholino-3-(4-morpholinophenyl)-3-phenyl-3*H*-naphtho[2,1-*b*]pyran (**3**)

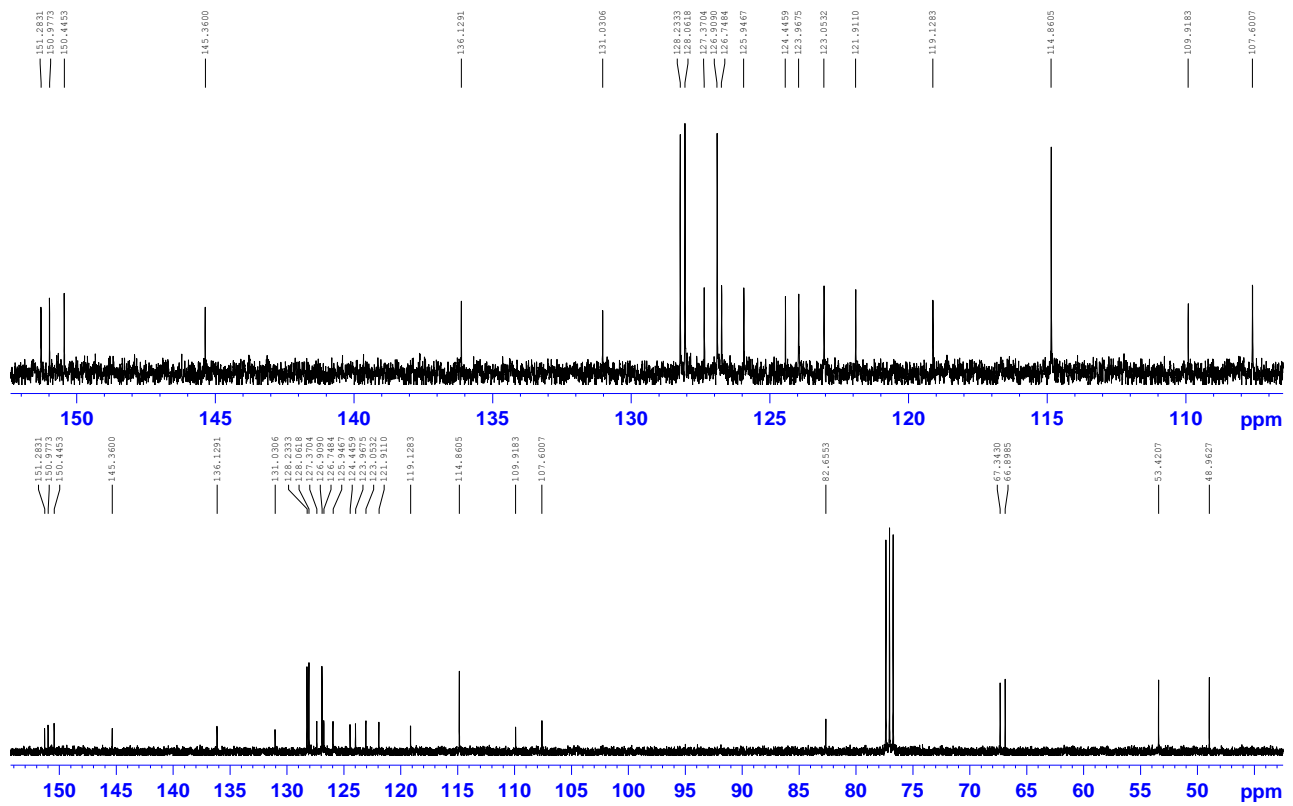
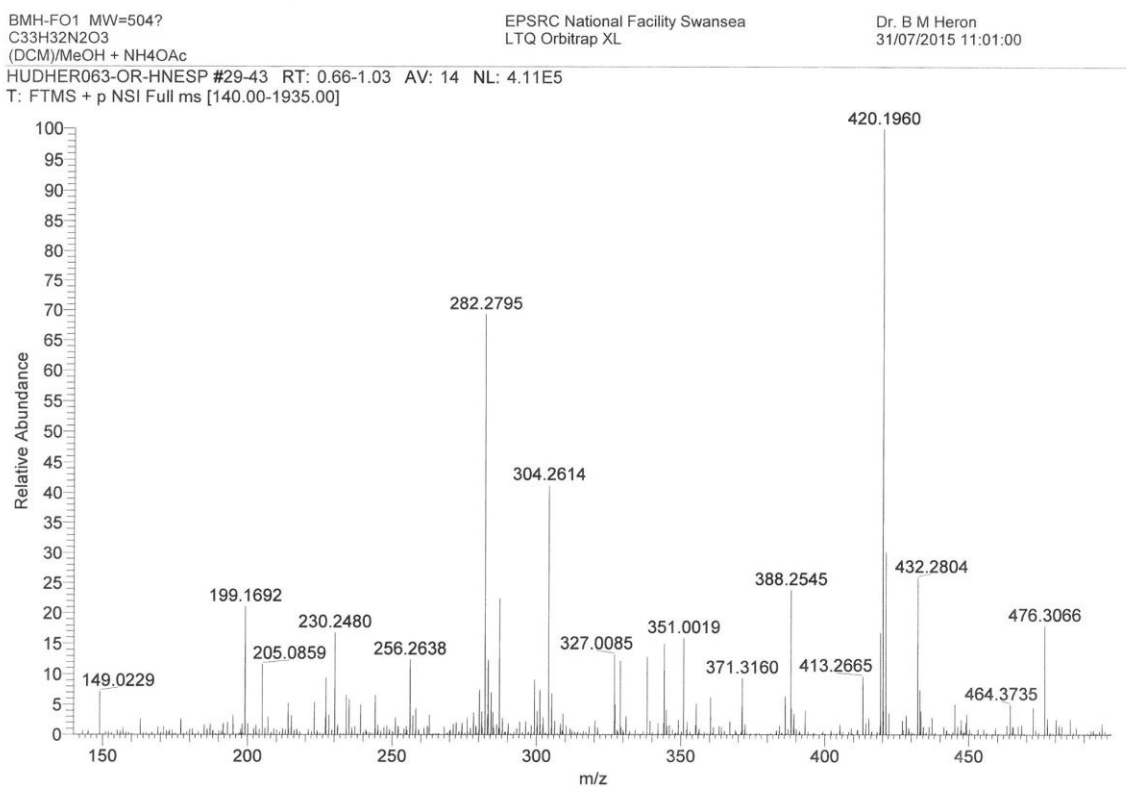
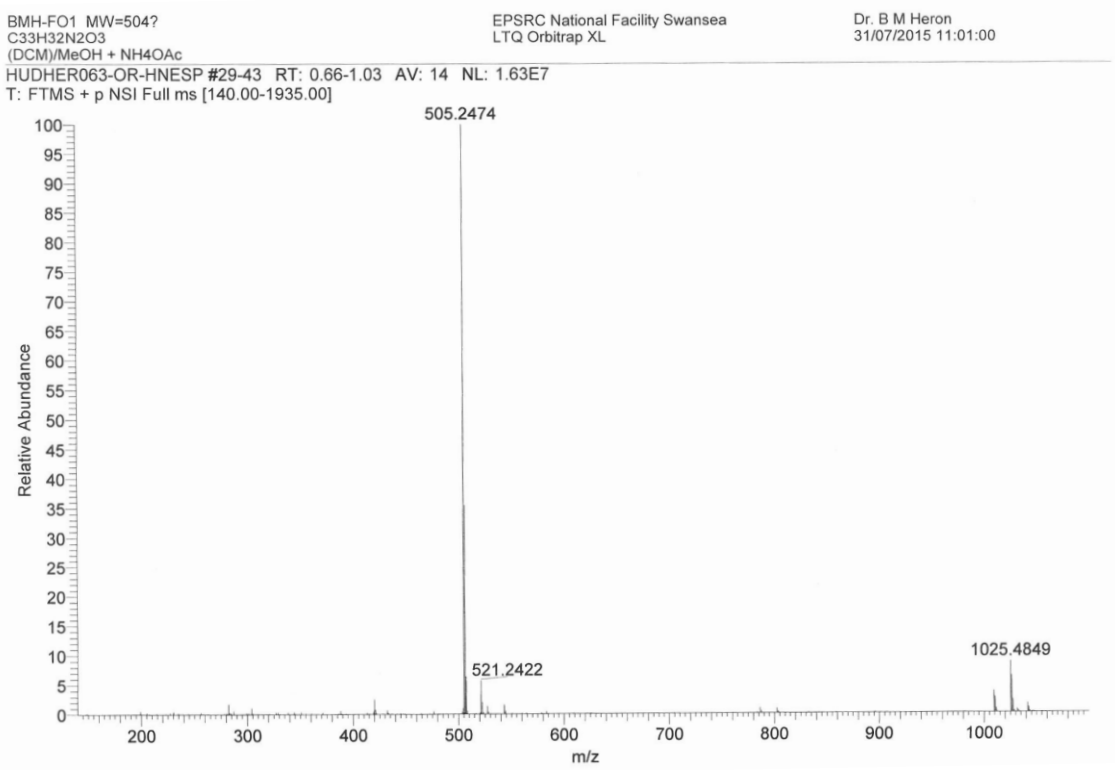


**Figure S7:** Mass Spectral data for 6-Morpholino-3-(4-morpholinophenyl)-3-phenyl-3*H*-naphtho[2,1-*b*]pyran (**3**)

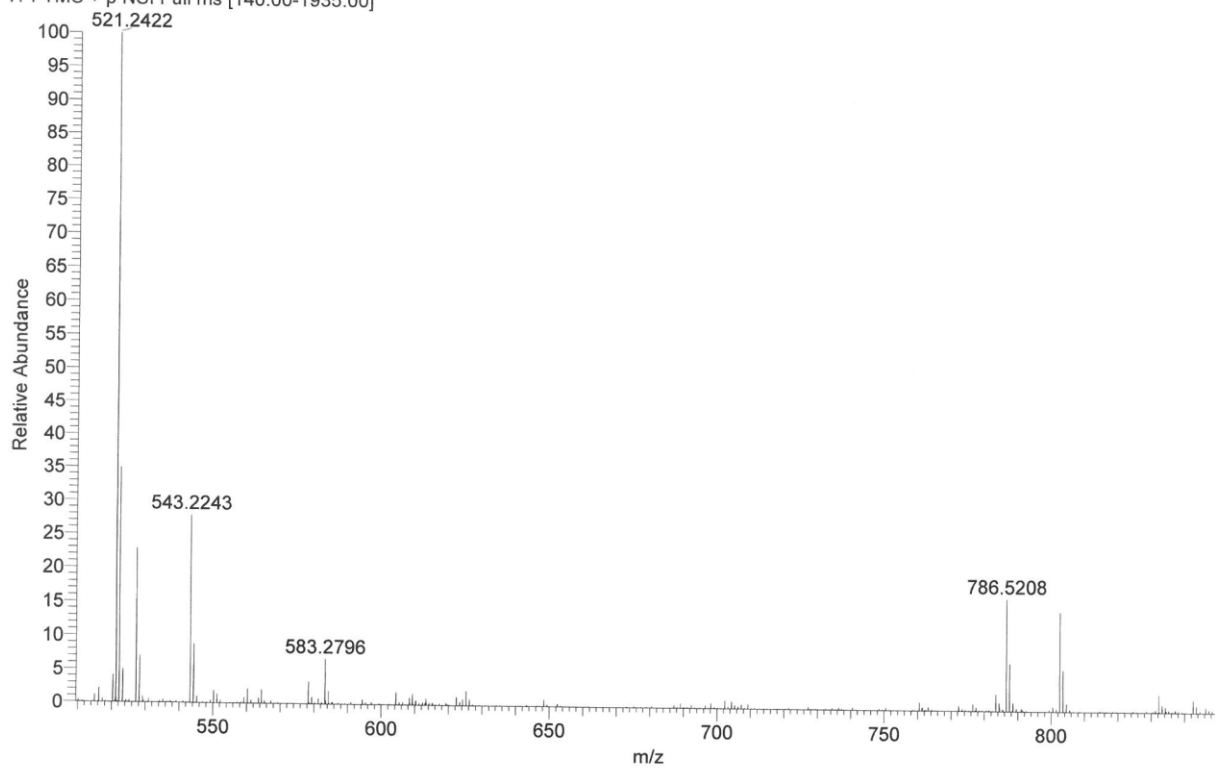


BMH-FO1 MW=504?  
C33H32N2O3  
(DCM)/MeOH + NH4OAc

EPSRC National Facility Swansea  
LTQ Orbitrap XL

Dr. B M Heron  
31/07/2015 11:01:00

HUDHER063-OR-HNESP #29-43 RT: 0.66-1.03 AV: 14 NL: 9.29E5  
T: FTMS + p NSI Full ms [140.00-1935.00]

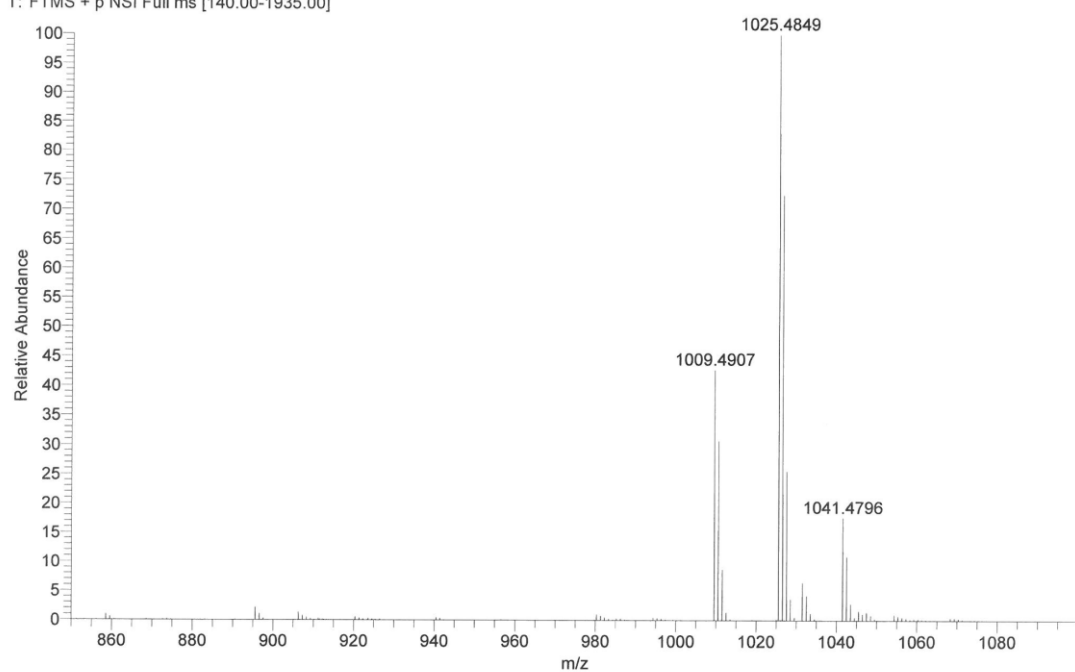


BMH-FO1 MW=504?  
C33H32N2O3  
(DCM)/MeOH + NH4OAc

EPSRC National Facility Swansea  
LTQ Orbitrap XL

Dr. B M Heron  
31/07/2015 11:01:00

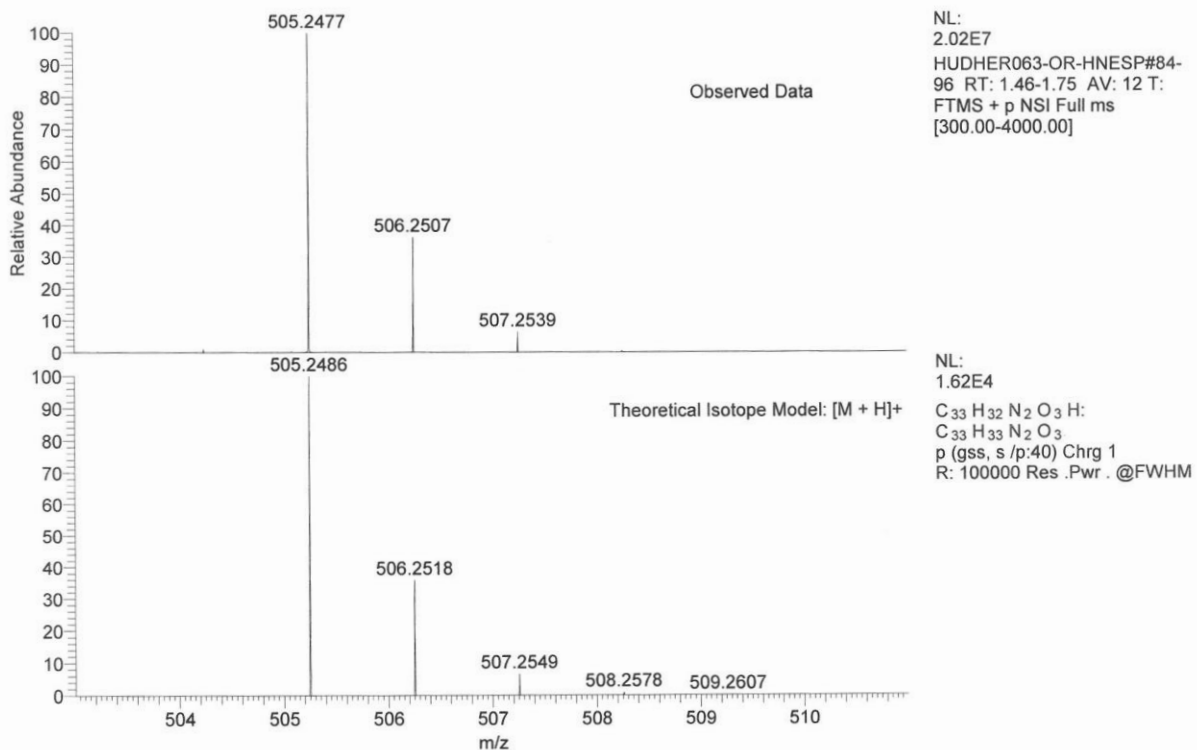
HUDHER063-OR-HNESP #29-43 RT: 0.66-1.03 AV: 14 NL: 1.42E6  
T: FTMS + p NSI Full ms [140.00-1935.00]



BMH-FO1 MW=504?  
C<sub>33</sub>H<sub>32</sub>N<sub>2</sub>O<sub>3</sub>  
(DCM)/MeOH + NH<sub>4</sub>OAc

EPSRC National Facility Swansea  
LTQ Orbitrap XL

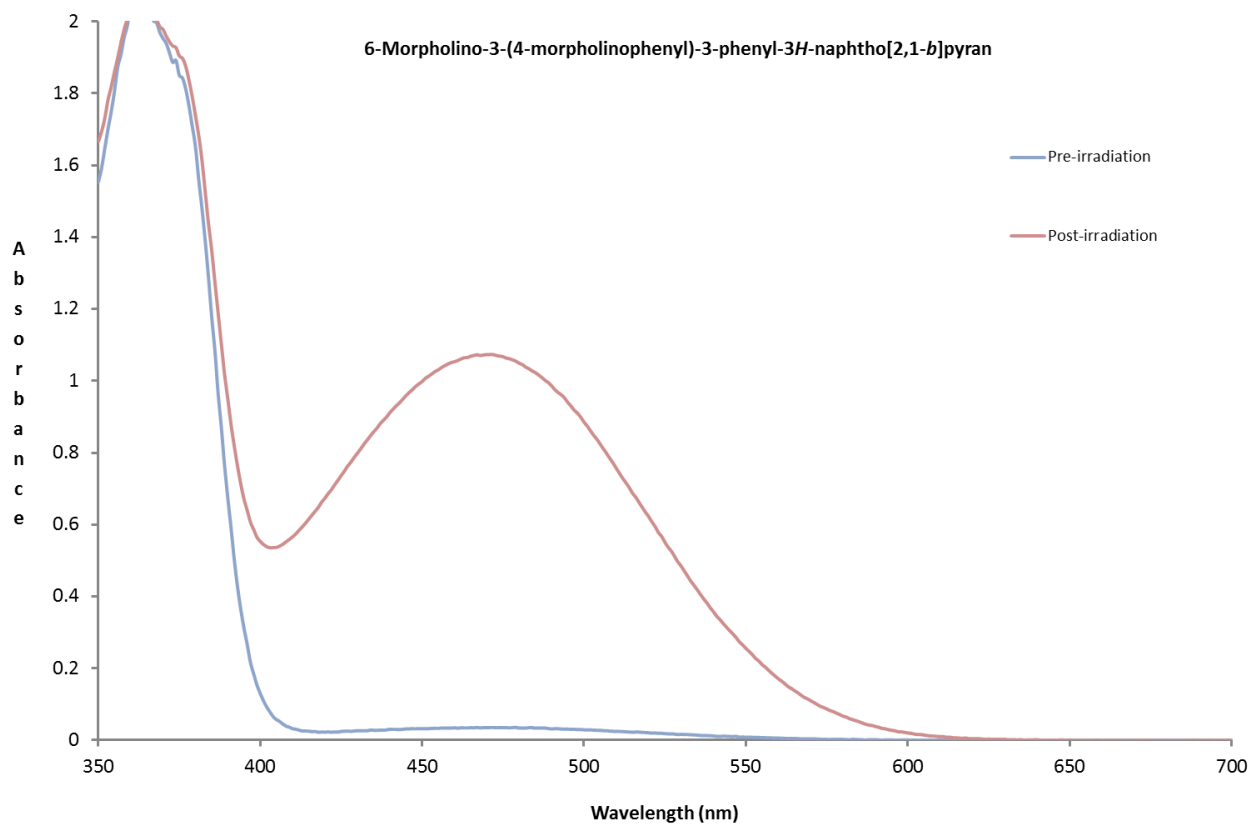
Dr. B M Heron  
31/07/2015 11:01:00



Isotope: Min. ... Max.  
14 N 0....10  
16 O 0....10  
12 C 0....60  
1 H 0....80  
23 Na 0....0  
Tolerance Window: +- 5.00 ppm  
Db/Ring Equiv: -3... 100 N-Rule: Do not use  
Fits: 100 Charge: 1

Mass	Theoretical Mass	Delta [ppm]	RDB	Composition
505.2477	505.2477	-0.1	6.5	C <sub>17</sub> H <sub>33</sub> O <sub>8</sub> N <sub>10</sub>
	505.2472	0.9	19.0	C <sub>31</sub> H <sub>31</sub> O <sub>2</sub> N <sub>5</sub>
	505.2486	-1.7	18.5	C <sub>13</sub> H <sub>33</sub> O <sub>3</sub> N <sub>2</sub>
	505.2491	-2.7	6.0	C <sub>19</sub> H <sub>35</sub> O <sub>9</sub> N <sub>7</sub>
	505.2459	3.6	14.0	C <sub>30</sub> H <sub>35</sub> O <sub>6</sub> N <sub>1</sub>
	505.2459	3.6	19.5	C <sub>29</sub> H <sub>29</sub> O <sub>1</sub> N <sub>8</sub>

**Figure S8:** UV-vis spectra of **3** before and after UV activation



#### Preparation of 3,3-Diphenyl-6-morpholino-3*H*-naphtho[2,1-*b*]pyran: **4**

A stirred solution of 4-morpholino-2-naphthol (1.50 g, 6.5 mmol) and 1,1-diphenylprop-2-yn-1-ol (1.36 g, 6.5 mmol) in toluene (75 mL) was warmed to 50 °C. Acidic alumina (4.0 g) was added and the mixture was heated under reflux until none of the prop-2-yn-1-ol remained by TLC (ca. 2.0 h). The mixture was cooled to ca. 50 °C and filtered and the alumina was washed with hot toluene (2 × 50 mL). Removal of the toluene from the combined washings and filtrate gave an orange-red gum that was eluted from silica with 50% EtOAc in *n*-hexane to afford the naphthopyran **4** 1.81 g, 65.7 % as pale yellow micro-crystals after crystallization from *n*-hexane / EtOAc, mp = 189 – 191 °C;  $\nu_{\max}$  2963, 2841, 2808, 1626, 1579, 1446, 1359, 1269, 1219, 1137, 1115, 1003, 922, 769, 741, 694, 513 cm<sup>-1</sup>;  $\delta_{\text{H}}$  3.10 – 3.11 (4H, m, N(CH<sub>2</sub>)<sub>2</sub>), 3.97 (4H, t, *J* = 4.5 Hz, O(CH<sub>2</sub>)<sub>2</sub>), 6.17 (1H, d, *J* = 9.9 Hz, 2-H), 6.86 (1H, s, 5-H), 7.24 – 7.29 (3H, m, Ar-H, 1-H), 7.31 – 7.36 (5H, m, Ar-H), 7.45 – 7.51 (5H, m, Ar-H), 7.96 (1H, d, *J* = 8.4 Hz, 7-H), 8.08 (1H, d, *J* = 7.9 Hz, 10-H);  $\delta_{\text{C}}$  55.4, 67.3, 82.8, 107.5, 110.0, 119.4, 121.9, 123.1, 124.0, 124.5, 125.8, 126.8, 127.0, 127.5, 128.1, 131.0, 145.1, 150.9, 151.4. Found [M+H]<sup>+</sup> = 420.1952, C<sub>29</sub>H<sub>25</sub>NO<sub>2</sub> requires [M+H]<sup>+</sup> = 420.1958.

**Figure S9:**  $^1\text{H}$  NMR Spectrum of 3,3-Diphenyl-6-morpholino-3*H*-naphtho[2,1-*b*]pyran (**4**)

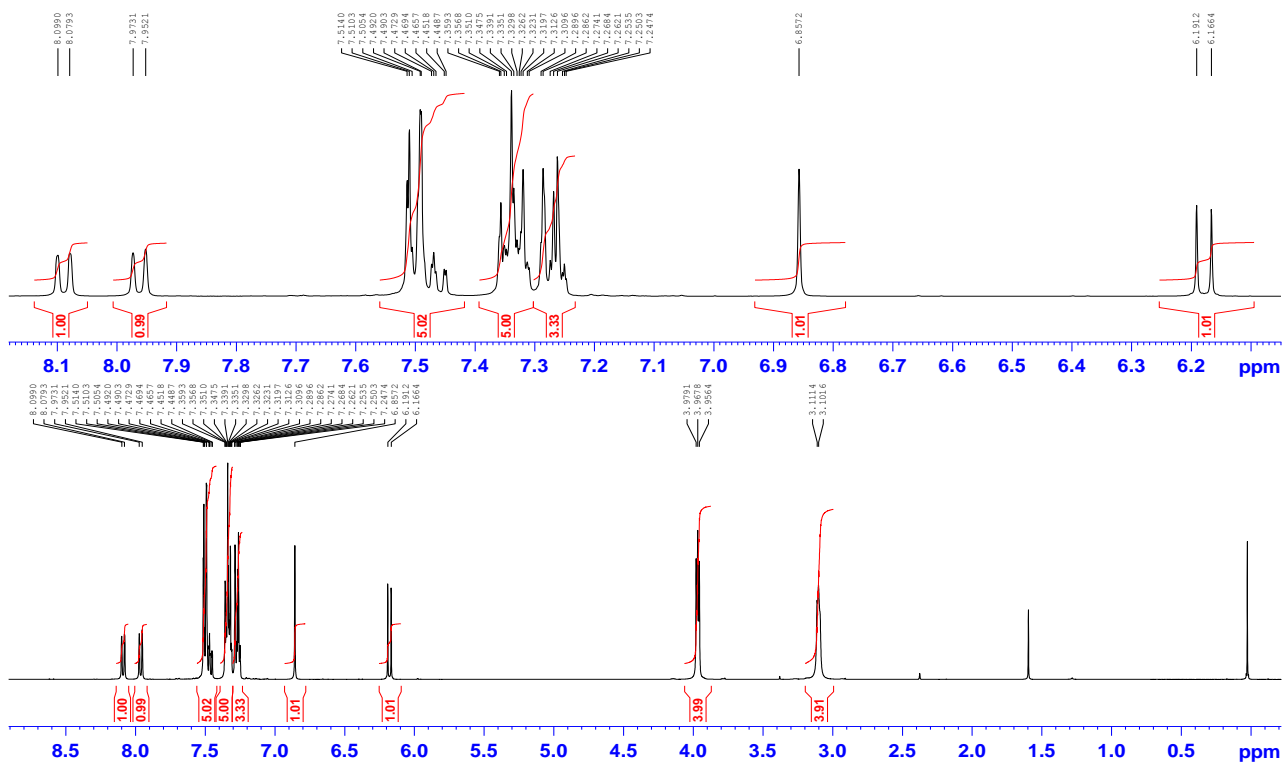


**Figure S10:**  $^{13}\text{C}$  NMR Spectrum of 3,3-Diphenyl-6-morpholino-3*H*-naphtho[2,1-*b*]pyran (**4**)

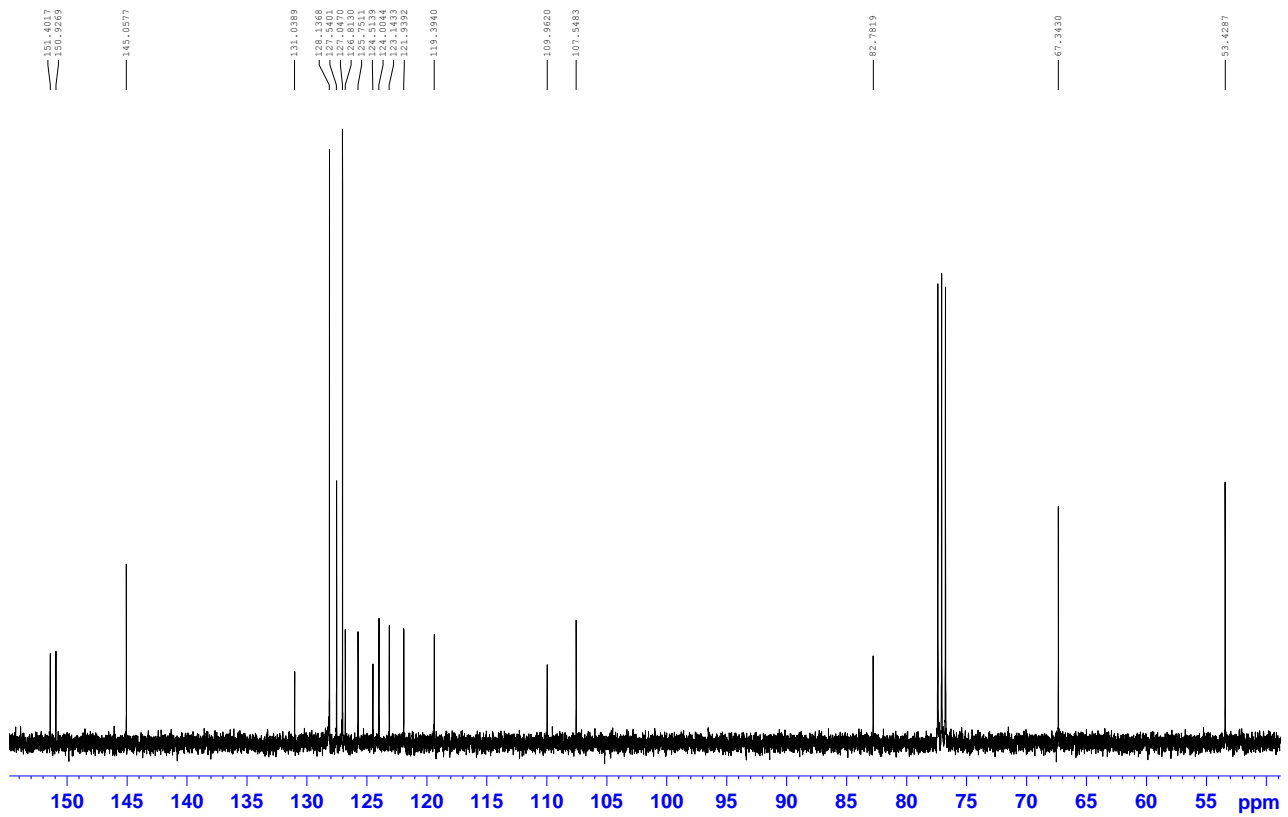
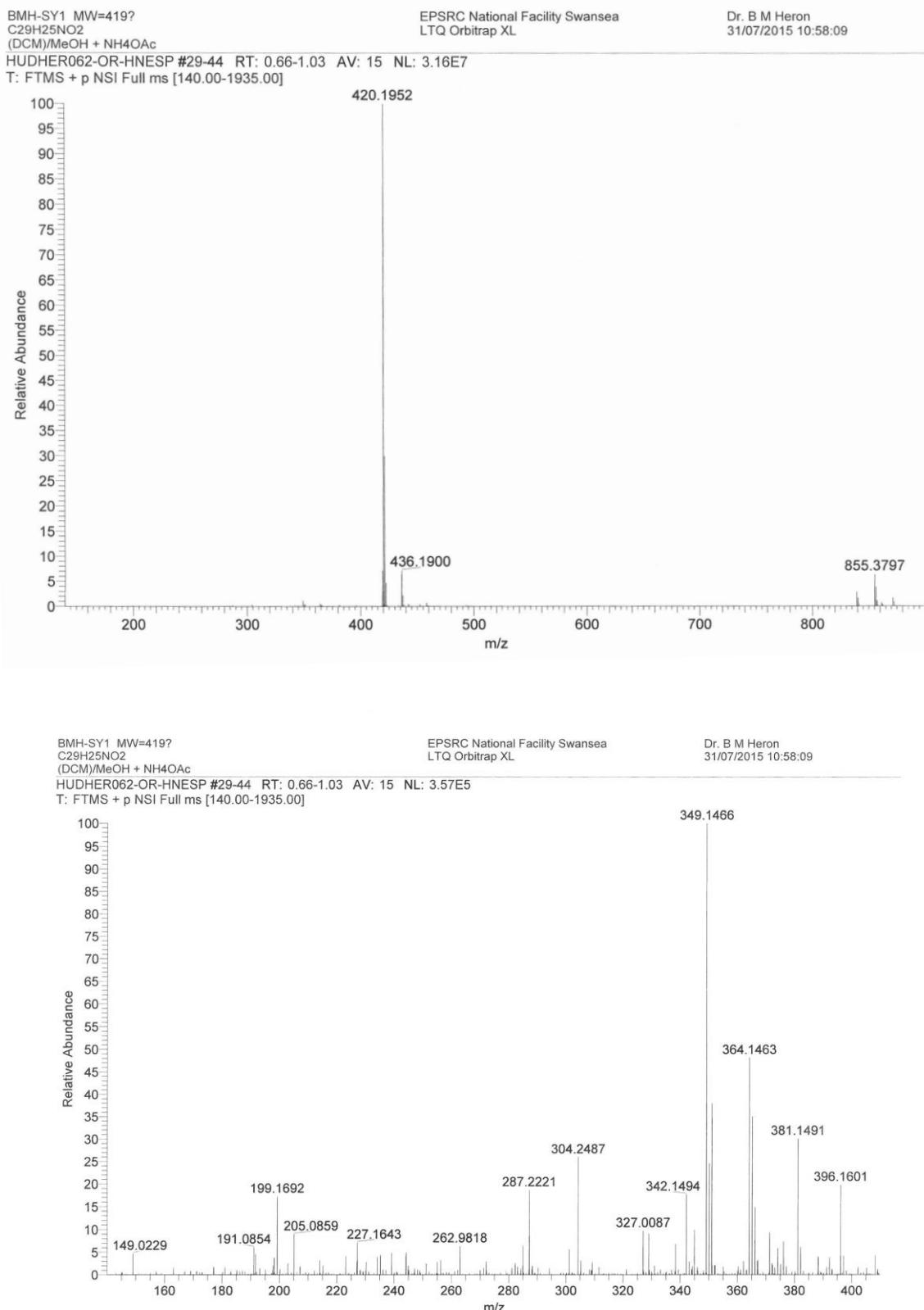


**Figure S11:** Mass Spectral data for 3,3-Diphenyl-6-morpholino-3*H*-naphtho[2,1-*b*]pyran (**4**)

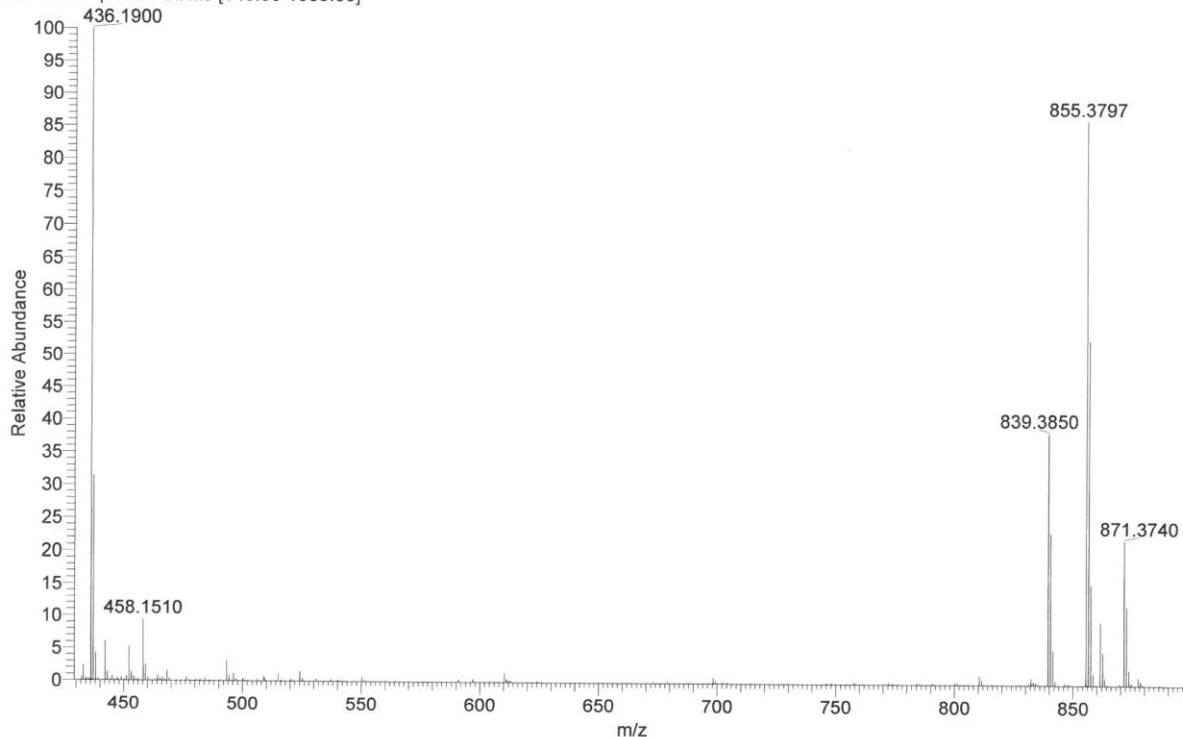


BMH-SY1 MW=419?  
C<sub>29</sub>H<sub>25</sub>NO<sub>2</sub>  
(DCM)/MeOH + NH<sub>4</sub>OAc

HUDHER062-OR-HNESP #29-44 RT: 0.66-1.03 AV: 15 NL: 2.27E6  
T: FTMS + p NSI Full ms [140.00-1935.00]

EPSRC National Facility Swansea  
LTQ Orbitrap XL

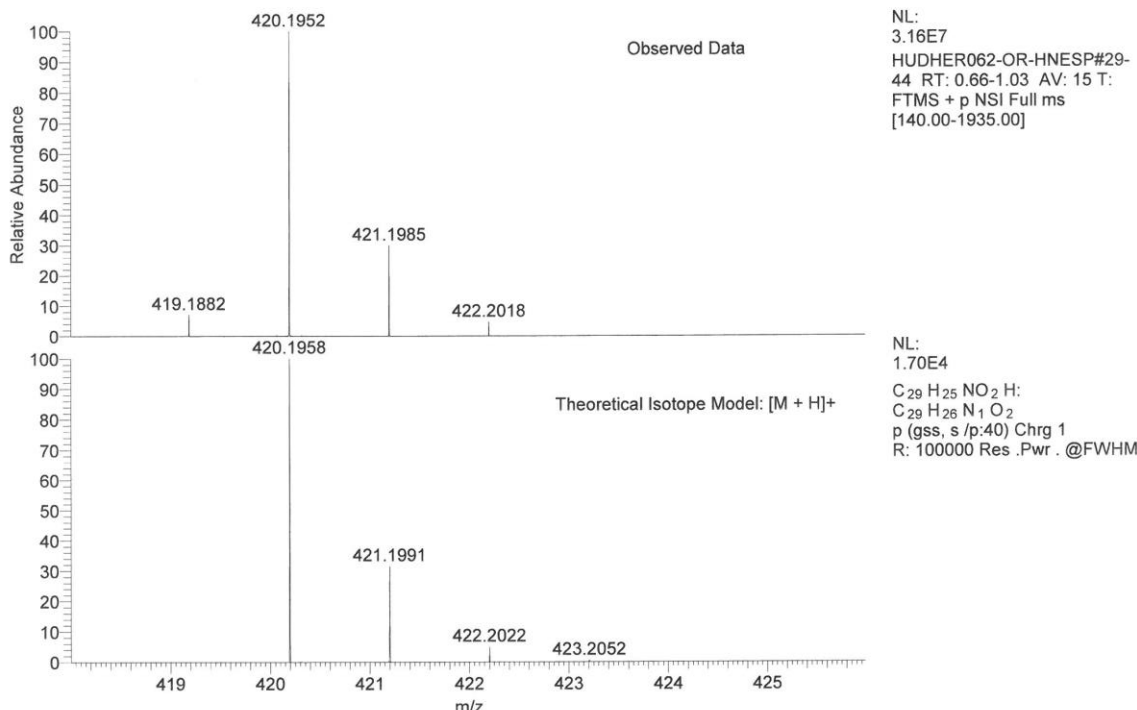
Dr. B M Heron  
31/07/2015 10:58:09



BMH-SY1 MW=419?  
C<sub>29</sub>H<sub>25</sub>NO<sub>2</sub>  
(DCM)/MeOH + NH<sub>4</sub>OAc

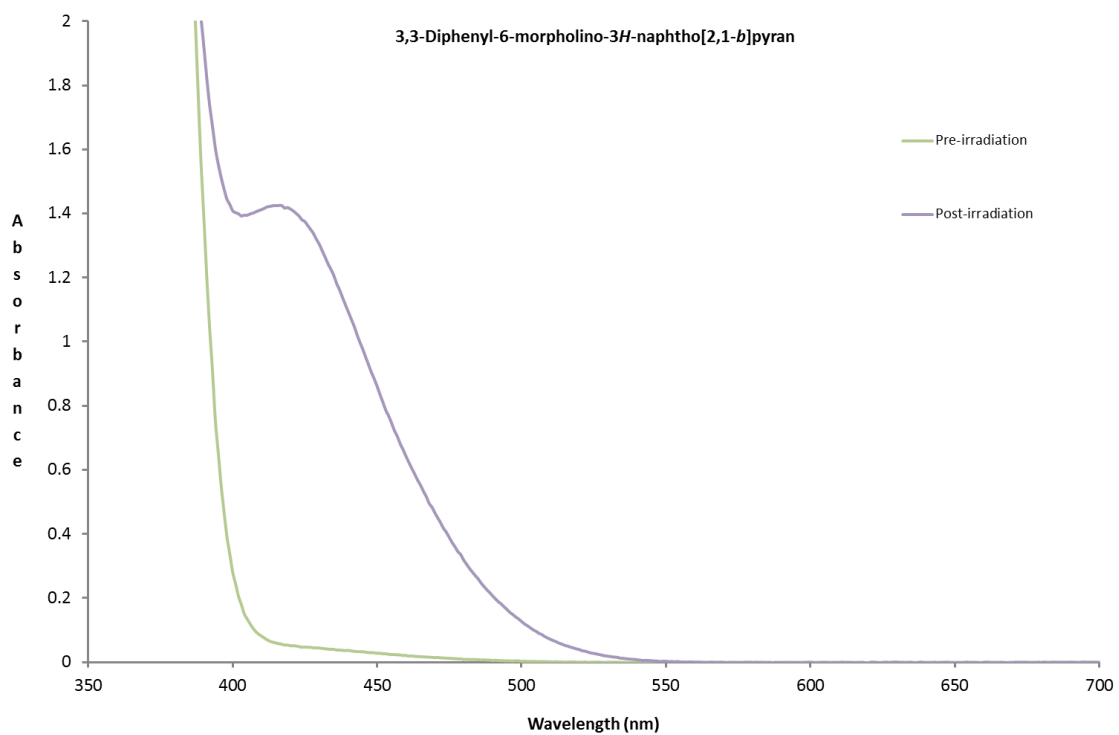
EPSRC National Facility Swansea  
LTQ Orbitrap XL

Dr. B M Heron  
31/07/2015 10:58:09



Isotope:	Min. . . Max.			
14 N	0....10			
16 O	0....10			
12 C	0....60			
1 H	0....80			
23 Na	0....0			
Tolerance Window:	+ - 5.00 ppm			
Db/Ring Equiv:	-3.. 100			
Fits:	100			
	N-Rule: Do not use			
	Charge: 1			
Mass	Theoretical Mass	Delta [ppm]	RDB	Composition
420.1952	420.1950	0.5	5.5	C <sub>13</sub> H <sub>26</sub> O <sub>7</sub> N <sub>9</sub>
	420.1958	-1.4	17.5	C <sub>29</sub> H <sub>26</sub> O <sub>2</sub> N <sub>1</sub>
	420.1945	1.8	18.0	C <sub>27</sub> H <sub>24</sub> O <sub>1</sub> N <sub>4</sub>
	420.1963	-2.6	5.0	C <sub>15</sub> H <sub>28</sub> O <sub>8</sub> N <sub>6</sub>
	420.1931	4.9	13.0	C <sub>26</sub> H <sub>28</sub> O <sub>5</sub>
	420.1931	4.9	18.5	C <sub>25</sub> H <sub>22</sub> N <sub>7</sub>

**Figure S12:** UV-vis spectra of **4** before and after UV activation



### **Preparation of 3-(2-Fluorophenyl)-3-(4-pyrrolidinophenyl)-3*H*-naphtho[2,1-*b*]pyran: 5**

A stirred solution of 2-naphthol (0.94 g, 6.5 mmol) and 1-(2-fluorophenyl)-1-(4-pyrrolidinophenyl)prop-2-yn-1-ol 1 (1.92 g, 6.5 mmol) in toluene (75 mL) was warmed to 50 °C. Acidic alumina (5.0 g) was added and the mixture was heated under reflux until none of the prop-2-yn-1-ol remained by TLC (ca. 1.5 h). The mixture was cooled to ca. 50 °C and filtered and the spent alumina catalyst was washed with hot toluene (3 × 40 mL). Removal of the toluene from the combined washings and filtrate gave a pale orange-red gum that was eluted from silica with 40% EtOAc in *n*-hexane to afford the naphthopyran **5** 1.04 g, 38 % as colourless micro-crystals after crystallization from *n*-hexane / EtOAc, mp 187.0 – 188.5 °C;  $\nu_{\text{max}}$  (KBr) 3039, 2962, 2831, 1612, 1520, 1483, 1352, 1194, 1153, 1091, 995, 807, 756, 732 cm<sup>-1</sup>;  $\delta_{\text{H}}$  1.96 (4H, t, *J* = 6.4 Hz, (CH<sub>2</sub>)<sub>2</sub>), 3.25 (4H, t, *J* = 6.3 Hz, N(CH<sub>2</sub>)<sub>2</sub>), 6.44 (1H, dd, *J* = 10.0, 4.6, 2-H), 6.49 (2H, m, Ar-H), 6.99 (1H, m, Ar-H), 7.11 (1H, m, Ar-H), 7.21 (1H, d, *J* = 8.9 Hz, 5-H), 7.24 – 7.33 (5H, m, Ar-H, 1-H), 7.46 (1H, m, Ar-H), 7.66 (1H, d, *J* = 8.8 Hz, 6-H), 7.71 – 7.76 (2H, m, Ar-H), 7.96 (1H, d, *J* = 8.5 Hz, 10-H);  $\delta_{\text{C}}$  25.5, 47.5, 81.2 (d, *J* = 3.1 Hz), 111.0, 113.7, 116.3 (d, *J* = 22.1 Hz), 118.3, 119.2, 121.4, 123.5, 123.6 (d, *J* = 3.4 Hz), 126.5, 126.6, 128.5, 129.2 (d, *J* = 8.3 Hz), 129.3, 129.6, 129.8, 130.0, 131.9 (d, *J* = 11.1 Hz), 147.5, 150.4, 159.1 (d, *J* = 246.4 Hz). Found [M+H]<sup>+</sup> = 422.1909, C<sub>29</sub>H<sub>24</sub>FNO requires [M+H]<sup>+</sup> = 422.1915.

**Figure S13:**  $^1\text{H}$  NMR Spectrum of 3-(2-Fluorophenyl)-3-(4-pyrrolidinophenyl)-3*H*-naphtho[2,1-*b*]pyran (**5**)

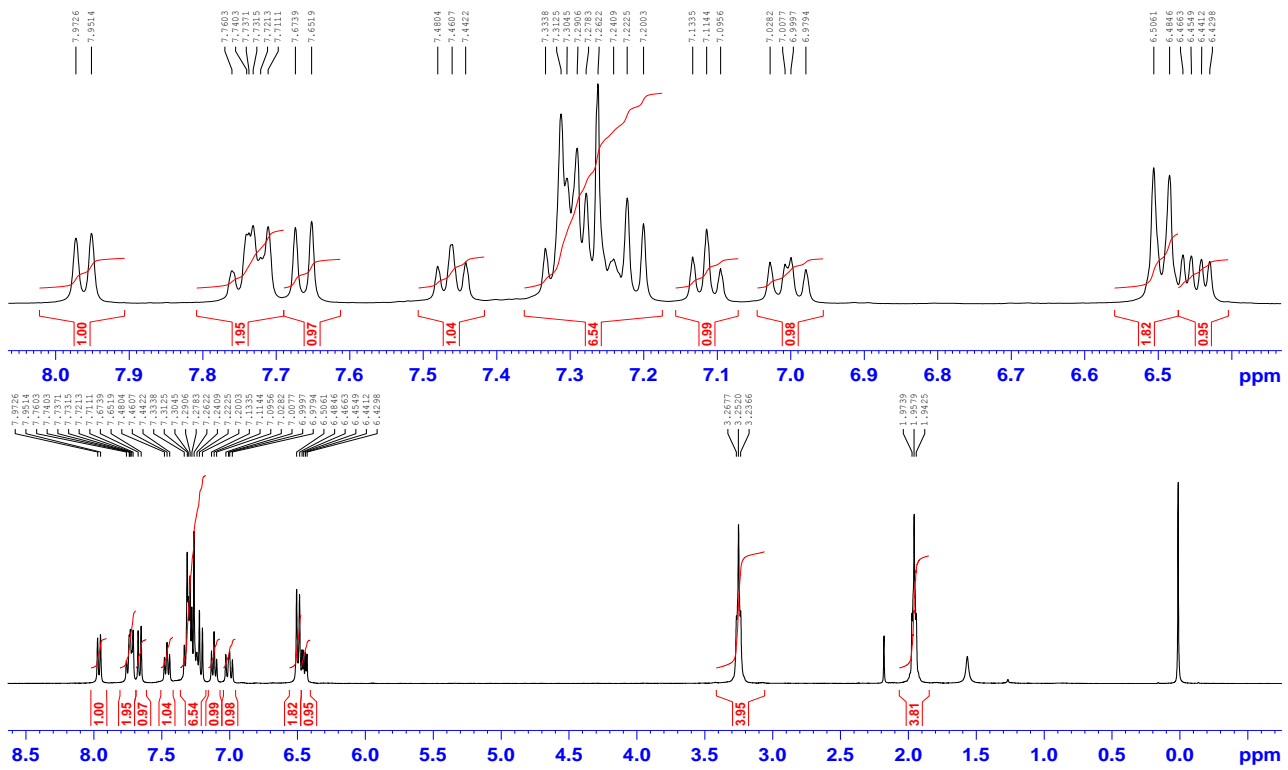


**Figure S14:**  $^{13}\text{C}$  NMR Spectrum of 3-(2-Fluorophenyl)-3-(4-pyrrolidinophenyl)-3*H*-naphtho[2,1-*b*]pyran (**5**)

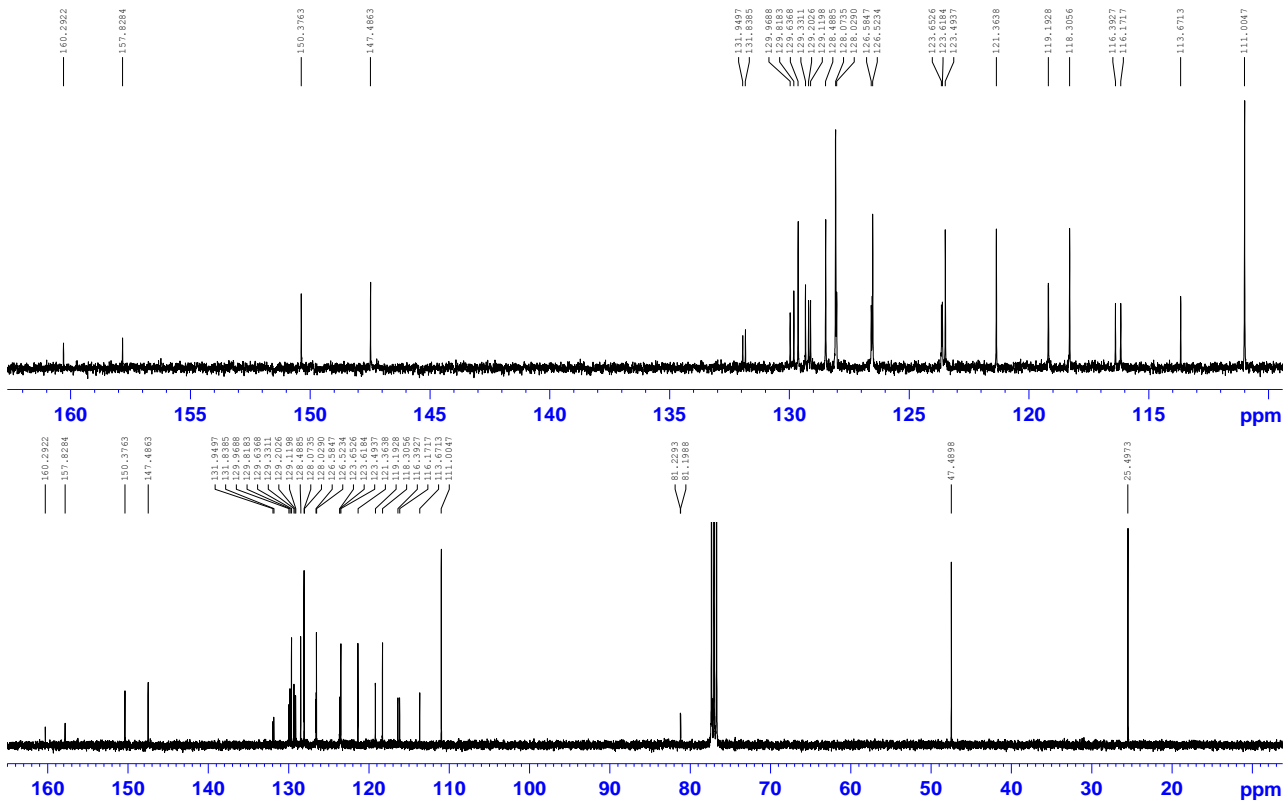
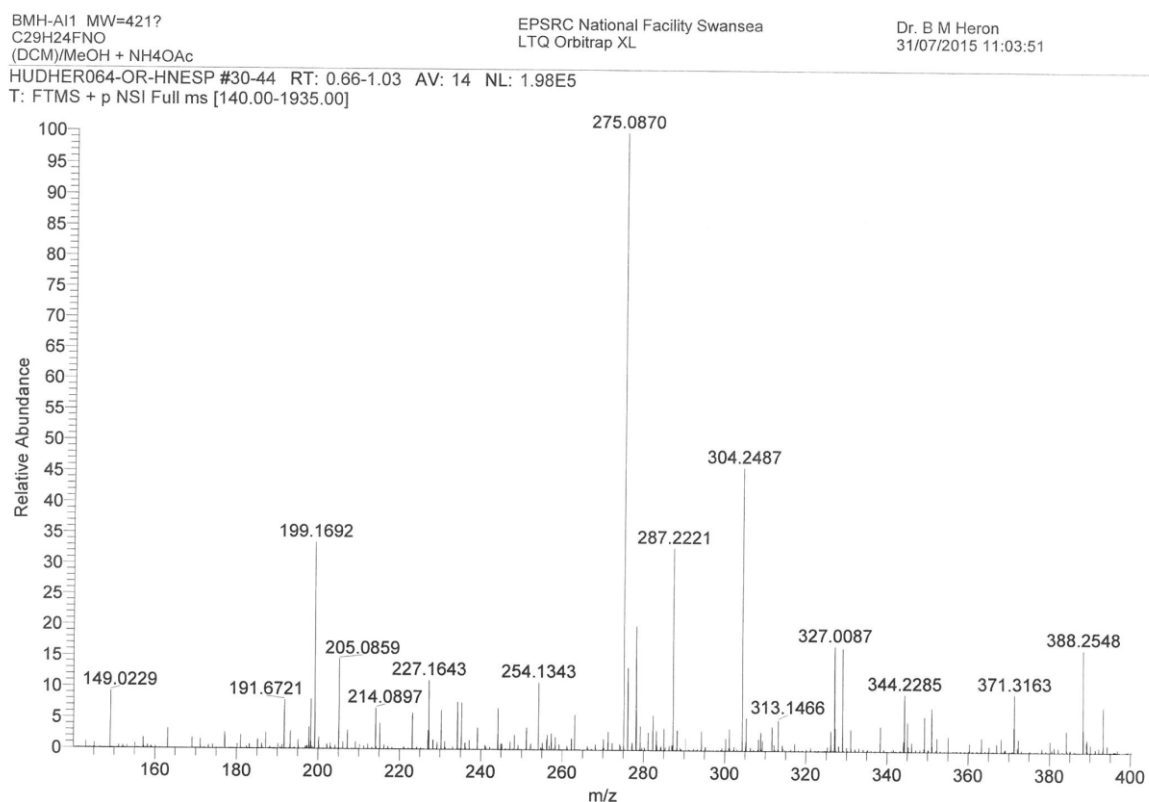
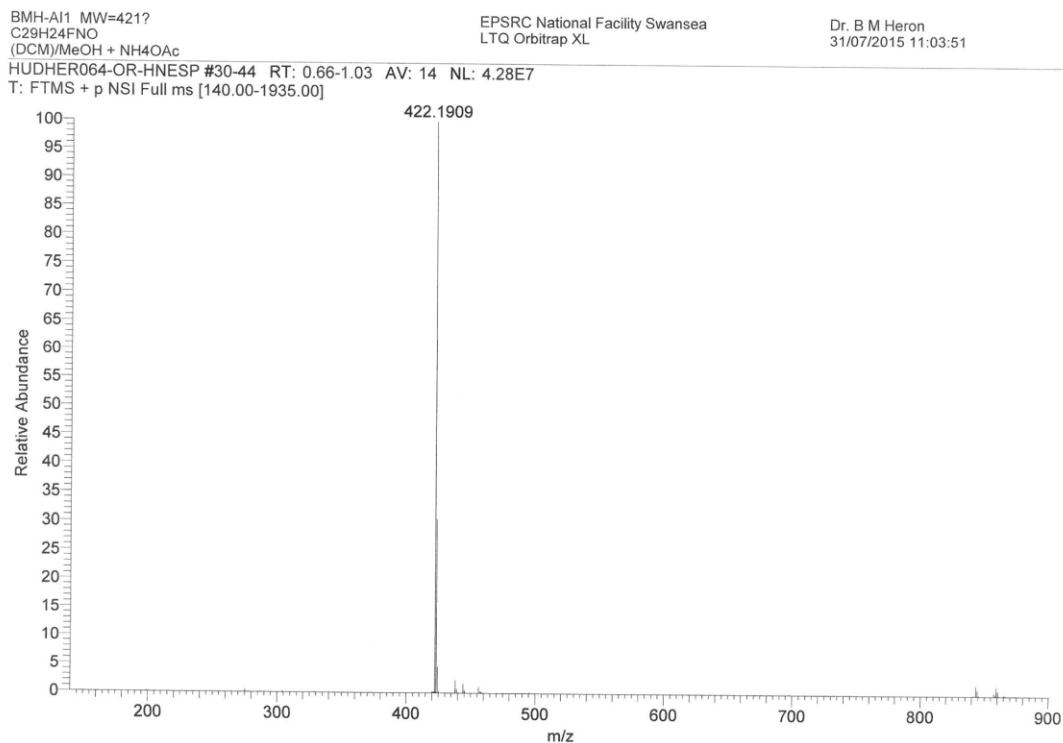


**Figure S15:** Mass Spectral data for 3-(2-Fluorophenyl)-3-(4-pyrrolidinophenyl)-3*H*-naphtho[2,1-*b*]pyran (**5**)

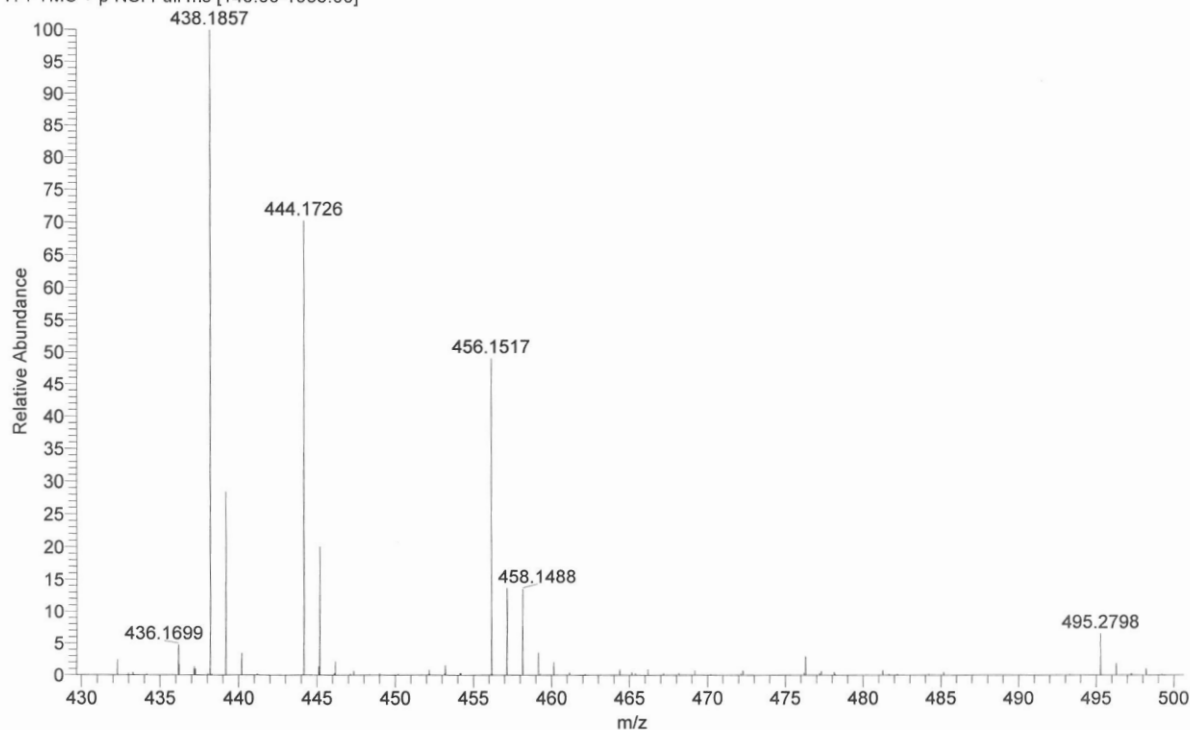


BMH-AI1 MW=421?  
C29H24FNO  
(DCM)/MeOH + NH4OAc

EPSRC National Facility Swansea  
LTQ Orbitrap XL

Dr. B M Heron  
31/07/2015 11:03:51

HUDHER064-OR-HNESP #30-44 RT: 0.66-1.03 AV: 14 NL: 9.69E5  
T: FTMS + p NSI Full ms [140.00-1935.00]

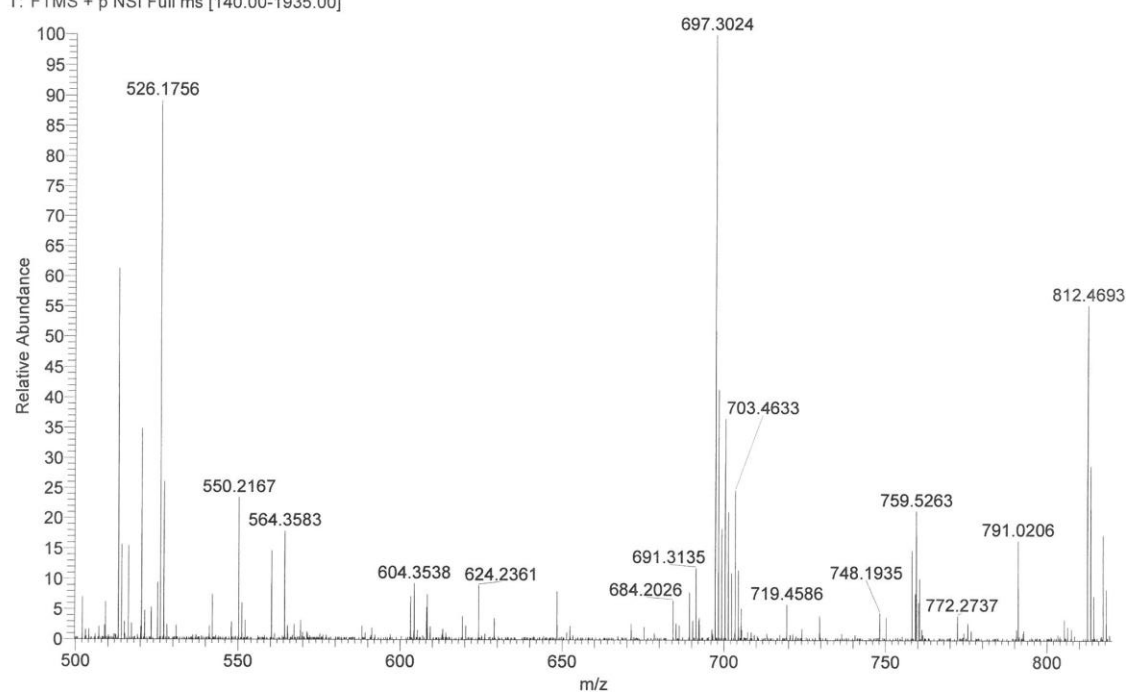


BMH-AI1 MW=421?  
C29H24FNO  
(DCM)/MeOH + NH4OAc

EPSRC National Facility Swansea  
LTQ Orbitrap XL

Dr. B M Heron  
31/07/2015 11:03:51

HUDHER064-OR-HNESP #30-44 RT: 0.66-1.03 AV: 14 NL: 4.23E4  
T: FTMS + p NSI Full ms [140.00-1935.00]

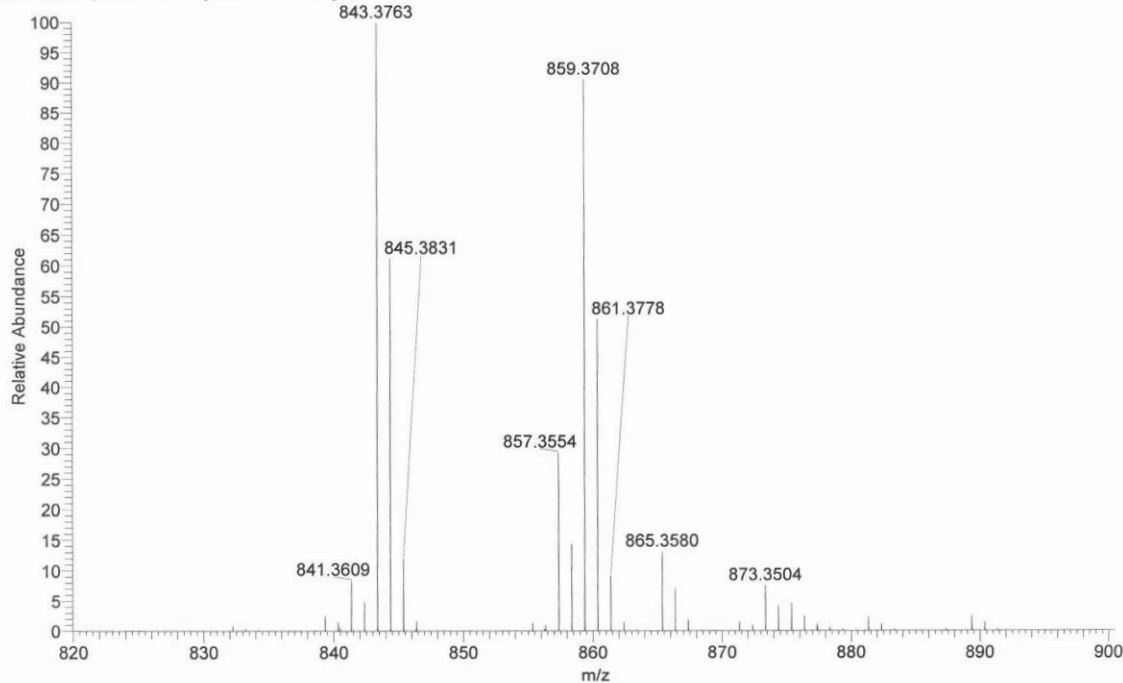


BMH-AI1 MW=421?  
C<sub>29</sub>H<sub>24</sub>FNO  
(DCM)/MeOH + NH<sub>4</sub>OAc

HUDHER064-OR-HNESP #30-44 RT: 0.66-1.03 AV: 14 NL: 7.63E5  
T: FTMS + p NSI Full ms [140.00-1935.00]

EPSRC National Facility Swansea  
LTQ Orbitrap XL

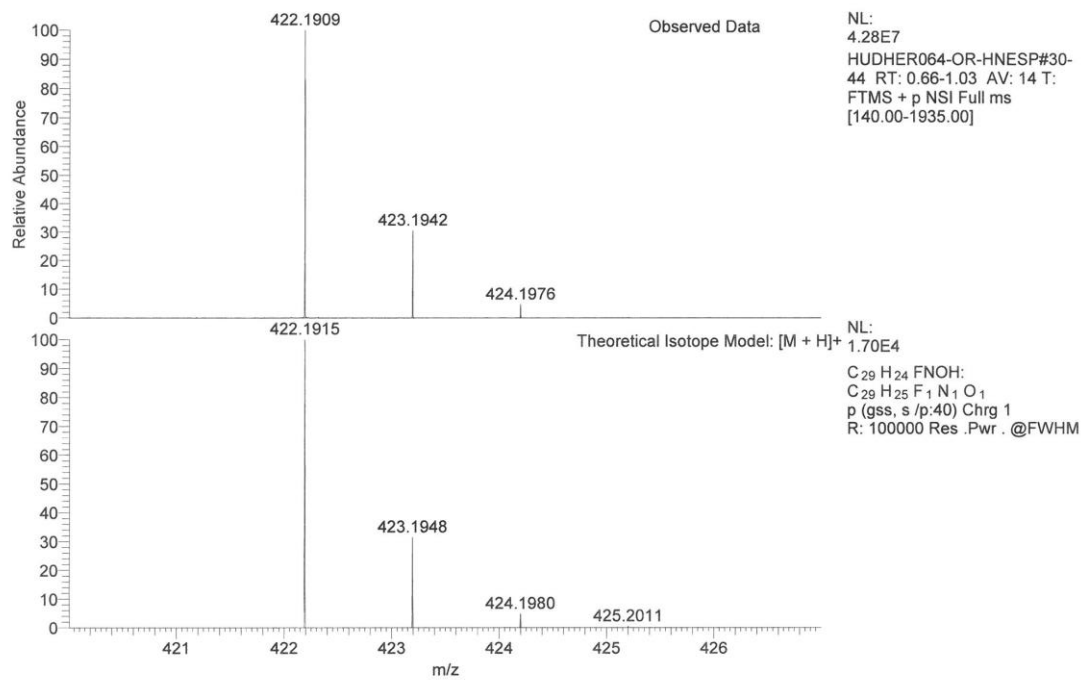
Dr. B M Heron  
31/07/2015 11:03:51



BMH-AI1 MW=421?  
C<sub>29</sub>H<sub>24</sub>FNO  
(DCM)/MeOH + NH<sub>4</sub>OAc

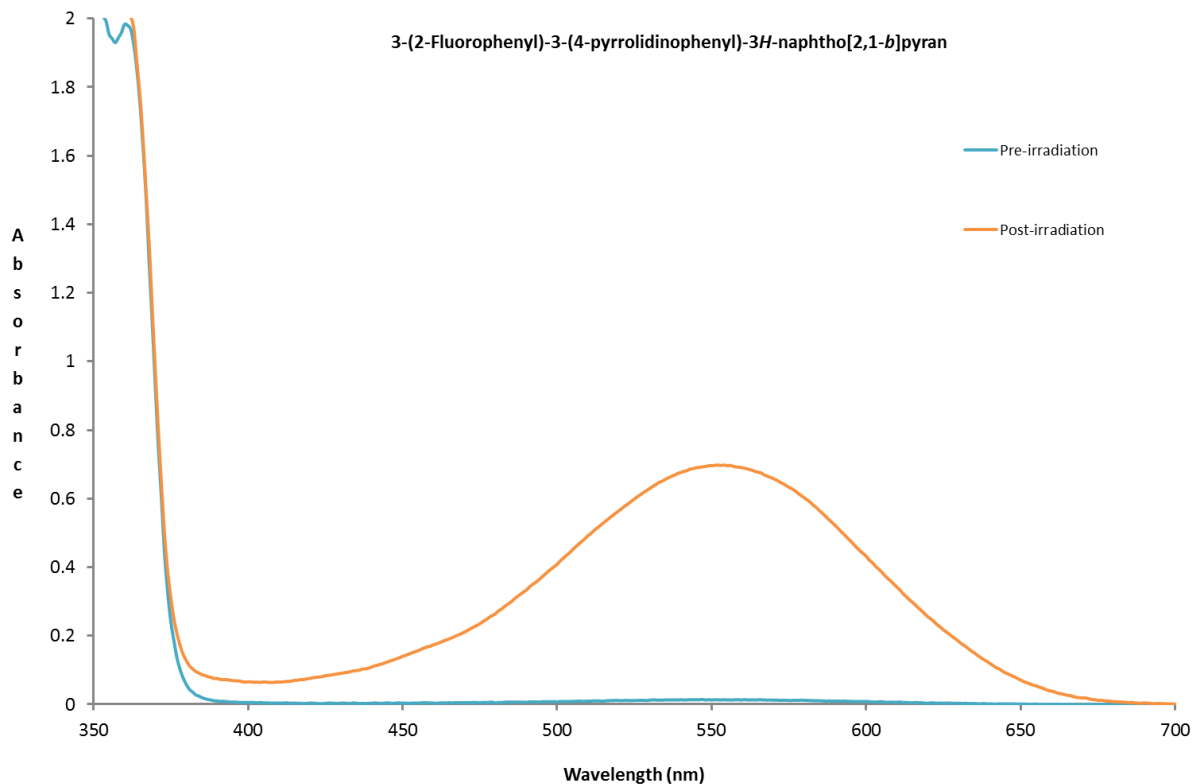
EPSRC National Facility Swansea  
LTQ Orbitrap XL

Dr. B M Heron  
31/07/2015 11:03:51



Isotope:		Min. . . Max.		
14 N		0....10		
16 O		0....10		
12 C		0....60		
1 H		0....80		
23 Na		0....0		
19 F		0....4		
Tolerance Window:		+ - 5.00 ppm		
Db/Ring Equiv:		-3.. 100	N-Rule:	Do not use
Fits:		100	Charge:	1
Mass	Theoretical Mass	Delta [ppm]	RDB	Composition
422.1909	422.1909	0.1	1.5	C <sub>15</sub> H <sub>28</sub> O <sub>6</sub> N <sub>4</sub> F <sub>4</sub>
	422.1909	0.1	7.0	C <sub>14</sub> H <sub>22</sub> O <sub>1</sub> N <sub>10</sub> F <sub>4</sub>
	422.1908	0.2	9.0	C <sub>18</sub> H <sub>26</sub> O <sub>6</sub> N <sub>6</sub>
	422.1911	-0.4	10.5	C <sub>19</sub> H <sub>23</sub> O <sub>1</sub> N <sub>6</sub> F <sub>3</sub>
	422.1911	-0.4	5.0	C <sub>20</sub> H <sub>29</sub> O <sub>6</sub> F <sub>3</sub>
	422.1906	0.6	5.5	C <sub>13</sub> H <sub>25</sub> O <sub>6</sub> N <sub>9</sub> F <sub>1</sub>
	422.1913	-0.9	14.0	C <sub>24</sub> H <sub>24</sub> O <sub>1</sub> N <sub>4</sub> F <sub>2</sub>
	422.1915	-1.3	17.5	C <sub>29</sub> H <sub>25</sub> O <sub>1</sub> N <sub>1</sub> F <sub>1</sub>
	422.1903	1.4	21.5	C <sub>12</sub> H <sub>25</sub> N <sub>1</sub>
	422.1901	1.8	18.0	C <sub>27</sub> H <sub>23</sub> N <sub>4</sub> F <sub>1</sub>
	422.1918	-2.1	1.5	C <sub>10</sub> H <sub>26</sub> O <sub>2</sub> N <sub>9</sub> F <sub>2</sub>
	422.1899	2.3	9.0	C <sub>23</sub> H <sub>28</sub> O <sub>9</sub> F <sub>2</sub>
	422.1899	2.3	14.5	C <sub>22</sub> H <sub>22</sub> N <sub>7</sub> F <sub>2</sub>
	422.1920	-2.6	5.0	C <sub>15</sub> H <sub>27</sub> O <sub>5</sub> N <sub>6</sub> F <sub>1</sub>
	422.1897	2.8	5.5	C <sub>18</sub> H <sub>27</sub> O <sub>5</sub> N <sub>3</sub> F <sub>3</sub>
	422.1897	2.8	11.0	C <sub>17</sub> H <sub>21</sub> N <sub>10</sub> F <sub>3</sub>
	422.1922	-3.0	14.0	C <sub>19</sub> H <sub>22</sub> O <sub>2</sub> N <sub>10</sub>
	422.1922	-3.0	8.5	C <sub>20</sub> H <sub>28</sub> O <sub>2</sub> N <sub>3</sub>
	422.1922	-3.1	6.5	C <sub>16</sub> H <sub>24</sub> O <sub>2</sub> N <sub>7</sub> F <sub>4</sub>
	422.1922	-3.1	1.0	C <sub>17</sub> H <sub>30</sub> O <sub>2</sub> N <sub>7</sub> F <sub>4</sub>
	422.1895	3.2	2.0	C <sub>13</sub> H <sub>26</sub> O <sub>5</sub> N <sub>6</sub> F <sub>4</sub>
	422.1895	3.3	4.0	C <sub>17</sub> H <sub>30</sub> O <sub>10</sub> N <sub>2</sub>
	422.1895	3.3	9.5	C <sub>16</sub> H <sub>24</sub> O <sub>2</sub> N <sub>9</sub>
	422.1924	-3.6	10.0	C <sub>21</sub> H <sub>25</sub> O <sub>2</sub> N <sub>4</sub> F <sub>3</sub>
	422.1893	3.8	0.5	C <sub>12</sub> H <sub>29</sub> O <sub>10</sub> N <sub>6</sub> F <sub>1</sub>
	422.1926	-4.1	13.5	C <sub>26</sub> H <sub>26</sub> O <sub>2</sub> N <sub>1</sub> F <sub>2</sub>
	422.1891	4.3	-3.0	C <sub>7</sub> H <sub>28</sub> O <sub>10</sub> N <sub>8</sub> F <sub>2</sub>
	422.1929	-4.8	-2.5	C <sub>7</sub> H <sub>27</sub> O <sub>8</sub> N <sub>9</sub> F <sub>3</sub>

**Figure S16:** UV-vis spectra of **5** before and after UV activation



**Experimental determinations of the photochemical quantum yields ( $\Phi_{PC}$ ) at different irradiation wavelengths in the UV, the bleaching kinetic constants ( $k_\Delta$ ) and the molar absorption coefficients of the coloured species.**

The absorption spectra, photo-coloration and bleaching kinetics were recorded with a Hewlett-Packard 8453 diode array spectrophotometer. A 125 W Xe lamp, filtered by a Jobin-Yvon H10 UV monochromator and focused on the sample through a 0.6 cm diameter silica optical fiber, was used as the irradiation source. A mercury lamp (Mineralight Compact 4-Watt UV lamp) was used to irradiate at 254 nm. The UV radiation ( $\lambda_{irr}$ ) emitted by 125 W Xe lamp, was focused on a 1 cm path length fluorimetric quartz cuvette, perpendicular to the monitoring beam of the spectrophotometer. The irradiation intensity was determined by potassium ferrioxalate actinometry and by performing spectro-radiometric measurements. For the latter measurements, we used an irradiance-calibrated AvaSpec-2048-2 spectrometer (Avantes, NL) provided with a 200 micrometer diameter optical fiber (FC-UVIR200-2ME, Avantes) and a 8 mm active area cosine corrector (CC-UV- VIS/NIR, Avantes). The spectroradiometer operates in the 171–1100 nm range (300 lines per mm grating) and is equipped with an AvaBench-75 optical bench, a 25 micrometer slit which produced 1.2 nm FWHM spectral resolution and a 2048 pixel CCD detector.

The differential equation describing how the absorbance into the visible changes over time due to the photo-production of the coloured species  $Co$  by UV irradiation of the uncoloured species  $Un$  is:

$$\frac{dA_{Co}}{dt} = \varepsilon_{Co} \Phi_{PC} I_{Un}^{\cdot} l - k_\Delta A_{Co} \quad (s.1)$$

wherein  $A_{Co}$  and  $\varepsilon_{Co}$  are the absorbance and the molar absorption coefficient of the coloured form, respectively;  $\Phi_{PC}$  is the quantum yield of the photoreaction,  $I_{Un}^{\cdot}$  is the intensity of the radiation absorbed by the uncoloured species,  $l$  is the optical path length and  $k_\Delta$  is the kinetic constant of the thermal bleaching reaction.  $I_{Un}^{\cdot}$  is defined by the following equation:

$$I_{Un}^{\cdot} = \frac{A_{Un}^{\cdot}}{A_{TOT}^{\cdot}} (1 - 10^{-A_{TOT}^{\cdot}}) I_0^{\cdot} = A_{Un}^{\cdot} F I_0^{\cdot} = \varepsilon_{Un}^{\cdot} l [Un] F I_0^{\cdot} = \varepsilon_{Un}^{\cdot} l (C_0 - [Co]) F I_0^{\cdot} \quad (s.2)$$

In equation (s.2),  $A_{Un}^{\cdot}$  is the absorbance value of the uncoloured species whose concentration is  $[Un]$  and whose absorption coefficient at the irradiation wavelength ( $\lambda_{irr}$ ) is  $\varepsilon_{Un}^{\cdot}$ ;  $A_{TOT}^{\cdot}$  represents the absorbance value at  $\lambda_{irr}$  due to both the uncoloured and the coloured species and the sum of their concentrations is  $[Un] + [Co] = C_0$ .  $I_0^{\cdot}$  is the intensity of the source at  $\lambda_{irr}$ , and  $F$  represents the photo-kinetic factor. When the irradiation is carried out at an isosbestic point for the photochromic system,  $F$  is constant over time. Inserting equation (s.2) into (s.1), we obtain equation (s.3):

$$\frac{dA_{Co}}{dt} = \varepsilon_{Co} l^2 \varepsilon_{Un}^{\cdot} \Phi_{PC} F I_0^{\cdot} C_0 - (k_\Delta + I_0^{\cdot} \Phi_{PC} F \varepsilon_{Un}^{\cdot} l) A_{Co} \quad (s.3)$$

After discontinuing the irradiation, the differential equation describing the spectral time evolution is:

$$\frac{dA_{Co}}{dt} = -k_{\Delta} A_{Co} \quad (s.4)$$

Equations (s.3) and (s.4) show that the first derivative of  $A_{Co}$  is linear in  $A_{Co}$  for both the colouration and the bleaching processes. By fitting the experimental data of the bleaching kinetics with equation (s.4), it has been possible to determine  $k_{\Delta}$ . On the other hand, by fitting the coloration kinetics with equation (s.3), we could estimate  $\Phi_{PC}$  and  $\varepsilon_{Co}$ , after evaluating  $I_0'$  by chemical actinometry and spectroradiometric measurements.

To determine the quantum yields at wavelengths different from the isosbestic point, the method of the initial rates was used. At the first instants of the photochemical reaction, the differential equation describing the spectral evolution is:

$$\frac{dA_{Co}}{dt} \approx \varepsilon_{Co} \Phi_{PC} I_0' l = \varepsilon_{Co} l \Phi_{PC} I_0' (1 - 10^{-A_{Tot}'}) \approx \varepsilon_{Co} l \Phi_{PC} I_0' (1 - 10^{-A_{TOT}'}) \quad (s.5)$$

The slope of the initial part (the first 10 seconds) of the photocolouration kinetics could be identified with the term on the right part of equation (s.5). After determining  $I_0'$  at the new  $\lambda_{irr}$ , knowing  $\varepsilon_{Co}$  and determining  $A_{TOT}'$  from the absorption spectrum, the photocolouration quantum yield  $\Phi_{PC}$  was estimated.

Below, we report the spectra recorded before UV irradiation and at the photo-stationary state, showing the isosbestic points. Moreover, we show graphs containing the application of the equations (s.3) and (s.4) for each photochromic compound.

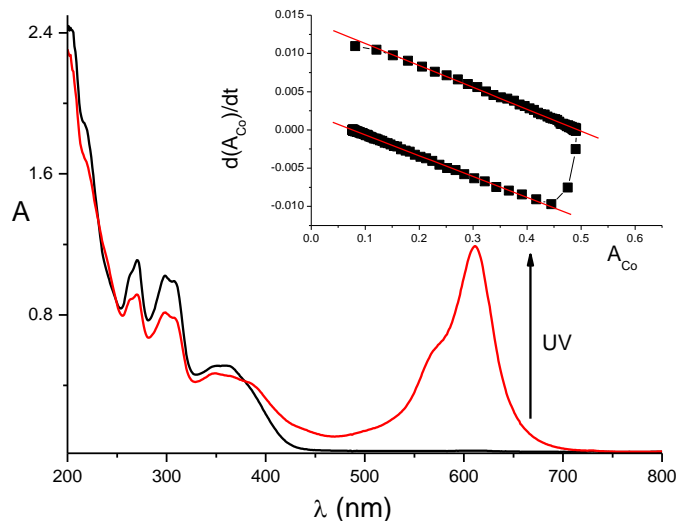


Figure S17: Spectra recorded for **1** before UV irradiation (black trace) and at the photo-stationary state (red trace). In the inset, kinetic treatment of the photo-colouration and bleaching processes recorded at 610 nm. The red straight lines represent the fitting functions shown in equations (s.3) and (s.4). It results that  $\Phi_{PC}$  at the isosbestic point (379 nm) is equal to 0.11.

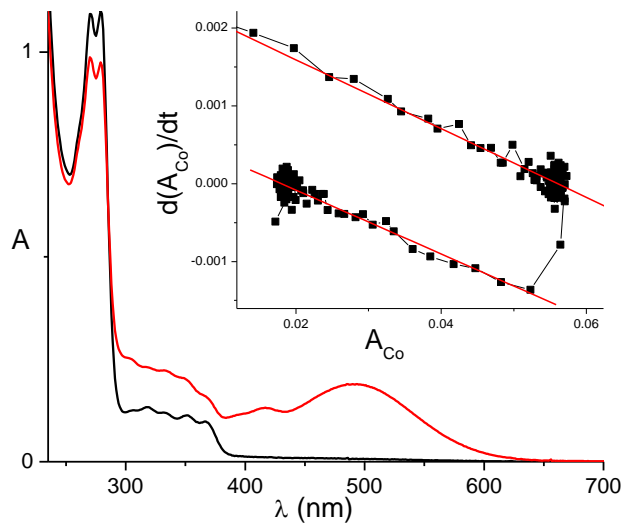


Figure S18: Effect of the UV irradiation on the spectrum of **2** (black trace). The red spectrum has been recorded at the photo-stationary state. **2** has an isosbestic point at 285 nm. In the inset, kinetic treatment of the photo-colouration and bleaching processes recorded at 490 nm. The red straight lines represent the fitting functions of equations (s.3) and (s.4). It results that  $\Phi_{PC}$ (for  $\lambda_{\text{irr}}=285 \text{ nm}$ )=0.12.

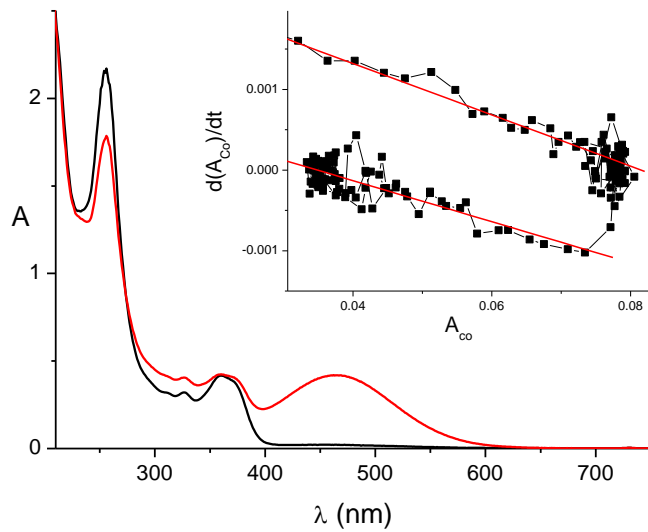


Figure S19: Effect of the UV irradiation on the spectrum of **3** (black trace). The red spectrum has been recorded at the photo-stationary state. **3** has an isosbestic point at 274 nm. In the inset, kinetic treatment of photo-colouration and bleaching processes recorded at 460 nm. The red straight lines represent the fitting functions of equations (s.3) and (s.4). It results that  $\Phi_{PC}$ (for  $\lambda_{\text{irr}}=274 \text{ nm}$ )=0.36.

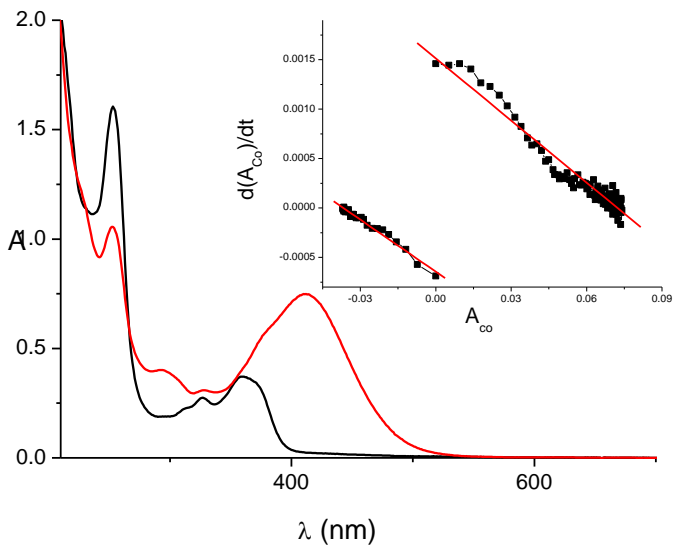


Figure S20: Effect of UV irradiation on the spectrum of **4** (black trace). The red spectrum has been recorded at the photo-stationary state. **4** has an isosbestic point at 266 nm. In the inset: kinetic treatment of photocolouration and bleaching processes recorded at 433 nm. The red straight lines represent the fitting functions of equations (s.3) and (s.4). It results that  $\Phi_{PC}$  for  $\lambda_{irr}=266$  nm is equal to 0.53.

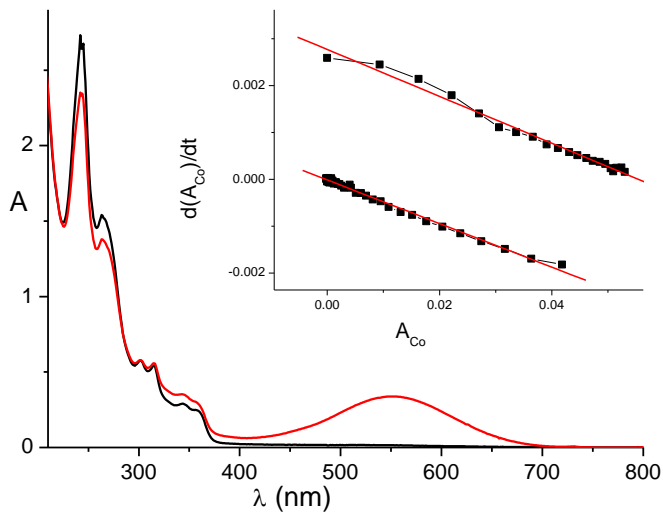


Figure S21: Effect of UV irradiation on the spectrum of **5** (black trace). The red spectrum has been recorded at the photostationary state. **5** has an isosbestic point at 285 nm. In the inset: kinetic treatment of photocolouration and bleaching processes recorded at 550 nm. The red straight lines represent the fitting functions of equations (s.3) and (s.4). It results that  $\Phi_{PC}$  for  $\lambda_{irr}=285$  nm is equal to 0.23.

## References

- S8. S. Delbaere, G. Vermeersch, J.-C. Micheau, Quantitative analysis of the dynamic behaviour of photochromic systems. *J. Photochem. Photobiol. C: Photochem. Rev.*, **2011**, 12, 74-105.

## Quantum mechanical simulations of the absorption spectra of the Uncoloured forms of 1 – 5.

The most stable conformations of the photochromic uncoloured forms have been determined by Density Functional Method (DFT) with STO-3G as basis set. The DFT method with 6-31G(d) as basis set has been used to simulate the absorption spectra of the uncoloured forms. In the simulations, the contribution of the solvent acetonitrile has been accounted for.

All the calculations have been performed by using Gaussian 03 as software.

### Results for 1

The geometry used for the simulation of the electronic absorption spectrum is the following:

Center Number	Atomic Number	Atomic Type	Coordinates (Angstroms)		
			X	Y	Z
1	6	0	2.217657	-3.711352	-0.564122
2	6	0	2.695699	-2.649208	0.218162
3	6	0	2.550976	-4.050269	2.180085
4	6	0	2.069440	-5.121490	1.415864
5	6	0	1.903690	-4.944832	0.033783
6	1	0	2.091047	-3.581384	-1.631062
7	1	0	2.937897	-1.701131	-0.242791
8	1	0	1.832112	-6.071226	1.876801
9	1	0	1.536142	-5.761244	-0.574165
10	7	0	3.321480	-1.902621	2.538900
11	6	0	2.848905	-2.848625	1.595172
12	6	0	4.010675	-0.664236	2.179529
13	1	0	3.373861	-0.060370	1.500478
14	1	0	4.219369	-0.061101	3.088313
15	1	0	4.970662	-0.903125	1.675960
16	6	0	3.418427	-2.536437	3.859844
17	6	0	2.822892	-4.008887	3.658480
18	6	0	3.839858	-5.113010	4.026778
19	1	0	4.761347	-5.027176	3.410913
20	1	0	4.116983	-5.036239	5.100080
21	1	0	3.411331	-6.123575	3.853092
22	6	0	1.503243	-4.276604	4.420653
23	1	0	1.659342	-4.170694	5.515654
24	1	0	0.704837	-3.575533	4.096178
25	1	0	1.137990	-5.308220	4.227031
26	6	0	2.598649	-1.691696	4.829755
27	1	0	1.580083	-1.432923	4.571311
28	7	0	3.079026	-1.258655	5.950103
29	6	0	4.420077	-1.522556	6.347851
30	6	0	4.899620	-1.094084	7.600239
31	6	0	5.270527	-2.192509	5.460516
32	6	0	6.238373	-1.348471	7.956878
33	6	0	6.600287	-2.433584	5.820508
34	6	0	7.083684	-2.018091	7.063249
35	1	0	7.260269	-2.948843	5.134307
36	1	0	8.115420	-2.216704	7.326272
37	8	0	4.823690	-2.619435	4.200415
38	6	0	4.033162	-0.376080	8.562264
39	1	0	2.999978	-0.162714	8.318087
40	6	0	4.516891	0.018855	9.745887
41	1	0	3.860021	0.542360	10.428841
42	6	0	5.929452	-0.247609	10.132801
43	6	0	6.738819	-0.899030	9.273891
44	1	0	7.769750	-1.101755	9.537365
45	7	0	6.417548	0.191897	11.415928
46	8	0	5.660279	0.793941	12.204872
47	8	0	7.599633	-0.019918	11.759126

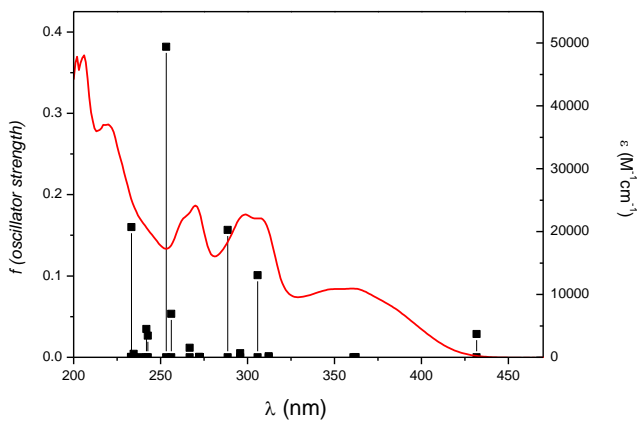
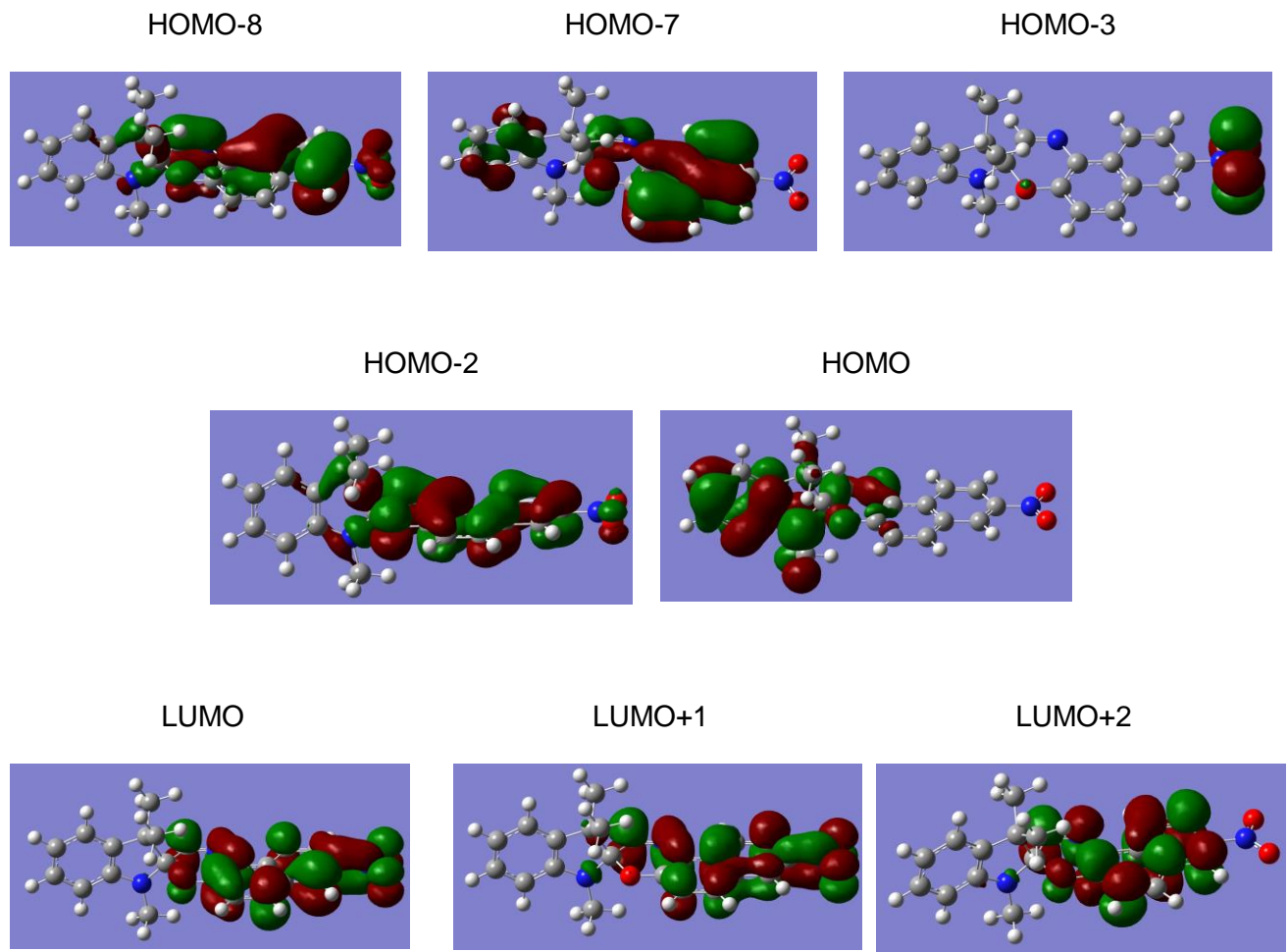


Figure S22: Electronic absorption spectrum of **1** (red trace) compared with the simulated oscillator strengths of the optically active transitions (vertical segments ending with a squared black dot).

Table S1: The principal optically active transitions of **1**, simulated by DFT 6-31G including the contribution of acetonitrile.

$\lambda$ (nm)	f(oscillator strength)	Orbitals	Weighting
431.73	0.0287	HOMO $\rightarrow$ LUMO	0.65477
		HOMO $\rightarrow$ LUMO+1	0.21481
305.76	0.1009	HOMO-2 $\rightarrow$ LUMO	0.63173
288.61	0.1565	HOMO-7 $\rightarrow$ LUMO	-0.28222
		HOMO-3 $\rightarrow$ LUMO	-0.11786
253.30	0.3817	HOMO-7 $\rightarrow$ LUMO	0.54441
		HOMO-7 $\rightarrow$ LUMO+1	-0.15244
		HOMO-2 $\rightarrow$ LUMO+1	0.23057
		HOMO-2 $\rightarrow$ LUMO+2	0.23091
233.20	0.1600	HOMO-8 $\rightarrow$ LUMO	-0.13243
		HOMO-8 $\rightarrow$ LUMO	-0.10923
		HOMO-7 $\rightarrow$ LUMO+1	0.47227

Figure S23: Molecular orbitals involved in the most optically active electronic transitions of **1**.



## Results for 2

The geometry used for the simulation of the electronic absorption spectrum is the following:

Center Number	Atomic Number	Atomic Type	Coordinates (Angstroms)		
			X	Y	Z
1	6	0	2.237390	-2.139361	0.310274
2	6	0	2.174841	-0.874881	-0.321746
3	6	0	3.377449	-0.258172	-0.726990
4	6	0	4.624379	-0.872135	-0.507466
5	6	0	4.682153	-2.138216	0.135336
6	6	0	3.468514	-2.765081	0.543121
7	1	0	1.300732	-2.619031	0.625091
8	1	0	3.344914	0.724724	-1.216903
9	1	0	5.537651	-0.363566	-0.832382
10	1	0	3.521298	-3.743075	1.038652
11	8	0	5.855044	-2.882505	0.431811
12	6	0	7.088820	-2.200531	-0.000198
13	1	0	7.915395	-2.876530	0.288663
14	1	0	7.119021	-2.043001	-1.098451
15	1	0	7.227933	-1.223302	0.507285
16	6	0	0.791592	-0.196526	-0.613713
17	6	0	0.819079	1.322829	-0.211646
18	6	0	0.407148	2.342342	-1.091970
19	6	0	1.228997	1.684857	1.098828
20	6	0	0.405472	3.696334	-0.702236
21	1	0	0.079236	2.076899	-2.106066
22	6	0	1.230011	3.021428	1.508999
23	1	0	1.548290	0.900465	1.798958
24	6	0	0.817636	4.050263	0.608869
25	1	0	0.080865	4.460107	-1.416063
26	1	0	1.545104	3.303714	2.521821
27	8	0	0.871201	5.359858	1.154117
28	6	0	0.423119	6.393406	0.202554
29	1	0	0.504647	7.351801	0.748844
30	1	0	1.065233	6.437787	-0.701682
31	1	0	-0.630947	6.245135	-0.111525
32	8	0	-0.174252	-0.884631	0.314216
33	6	0	-1.520495	-0.865295	-0.112814
34	6	0	-1.934202	-0.737668	-1.452571
35	6	0	-0.859374	-0.635874	-2.470288
36	1	0	-1.113048	-0.791963	-3.526172
37	6	0	0.415331	-0.409544	-2.100009
38	1	0	1.240571	-0.374471	-2.822292
39	6	0	-3.345973	-0.789350	-1.789360
40	6	0	-4.306264	-1.018622	-0.796898
41	6	0	-3.886620	-1.188719	0.590232
42	6	0	-2.490973	-1.109123	0.941292
43	6	0	-3.714008	-0.588593	-3.274614
44	1	0	-3.132490	0.241371	-3.704002
45	1	0	-3.490696	-1.496252	-3.861574
46	1	0	-4.777991	-0.354585	-3.404591
47	6	0	-5.814163	-1.116622	-1.097896
48	1	0	-6.211687	-2.089898	-0.765924
49	1	0	-6.373521	-0.328548	-0.566477
50	1	0	-6.025861	-1.019079	-2.169398
51	6	0	-2.078594	-1.266636	2.307825
52	1	0	-1.006298	-1.192802	2.533621
53	6	0	-3.012393	-1.502419	3.306472
54	1	0	-2.694324	-1.621848	4.350525
55	6	0	-4.399666	-1.585747	2.973029
56	1	0	-5.135615	-1.770681	3.767227
57	6	0	-4.822879	-1.432020	1.659131
58	1	0	-5.892308	-1.497105	1.428385

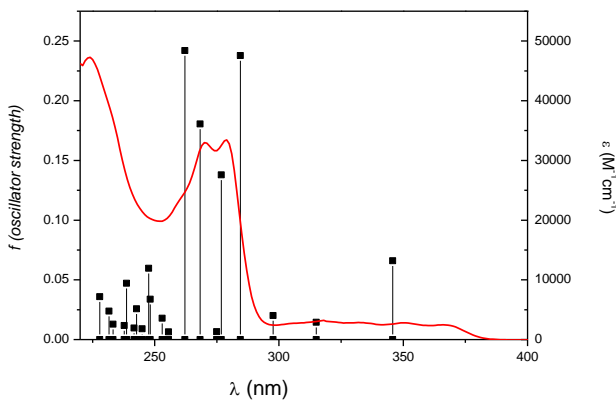
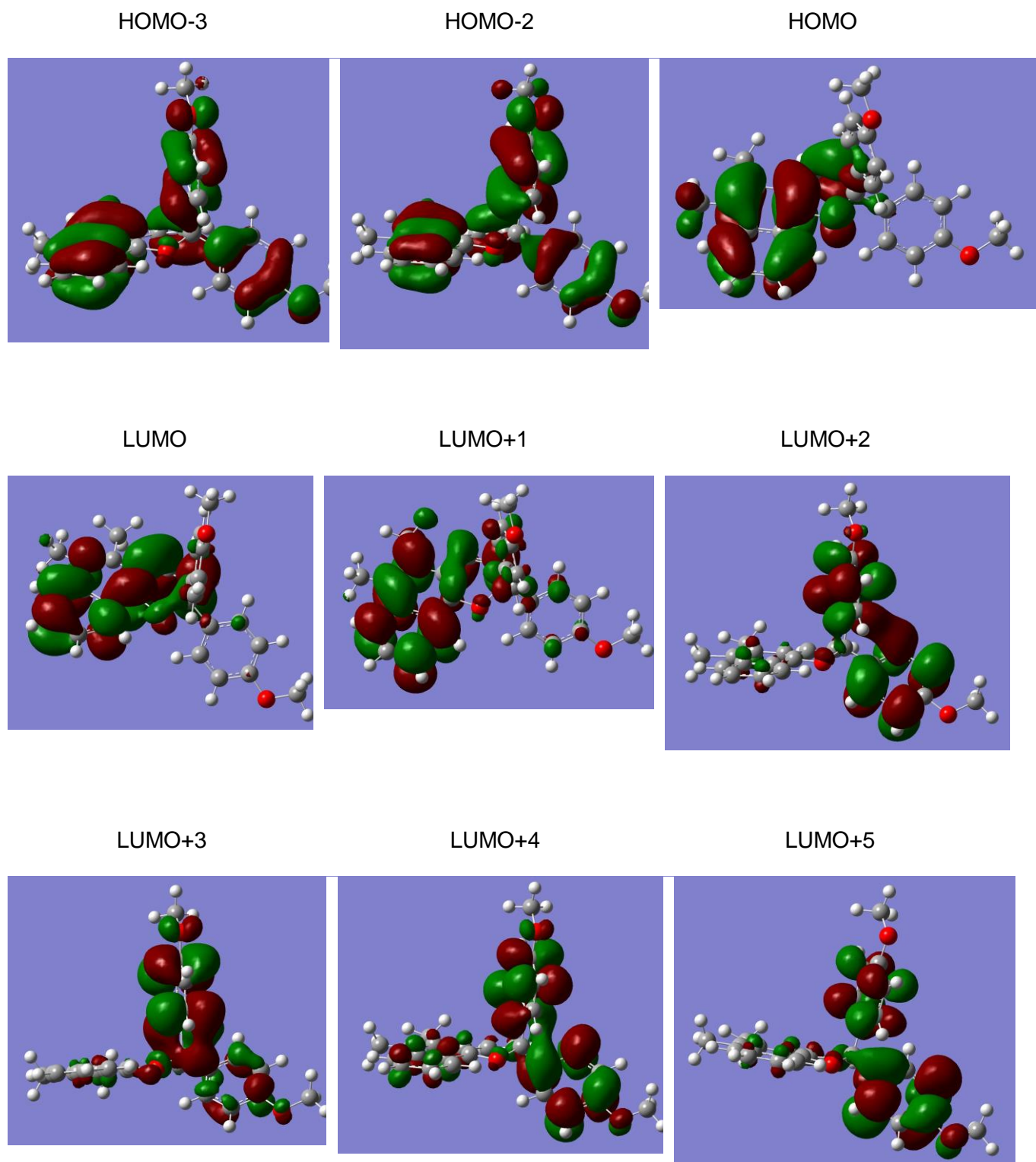


Figure S24: Electronic absorption spectrum of **2** (red trace) compared with the simulated oscillator strengths of the optically active transitions (vertical segments ending with a squared black dot).

Table S2: The principal optically active transitions of **2**, simulated by DFT 6-31G including the contribution of acetonitrile.

$\lambda$ (nm)	f(oscillator strength)	n° orbitals	Weightings
345.76	0.0660	HOMO $\rightarrow$ LUMO HOMO $\rightarrow$ LUMO+1	0.63613 0.12110
284.44	0.2379	HOMO-3 $\rightarrow$ LUMO HOMO-2 $\rightarrow$ LUMO HOMO $\rightarrow$ LUMO+1	-0.25424 0.59863 0.19408
276.81	0.1379	HOMO-3 $\rightarrow$ LUMO HOMO $\rightarrow$ LUMO+1 HOMO $\rightarrow$ LUMO+2 HOMO $\rightarrow$ LUMO+3 HOMO $\rightarrow$ LUMO+4	0.39874 0.22674 -0.39531 -0.26607 -0.14983
268.26	0.1805	HOMO-3 $\rightarrow$ LUMO HOMO $\rightarrow$ LUMO HOMO $\rightarrow$ LUMO+3 HOMO $\rightarrow$ LUMO+4	0.22250 0.11755 0.55607 -0.28568
262.17	0.2420	HOMO-3 $\rightarrow$ LUMO HOMO-2 $\rightarrow$ LUMO HOMO $\rightarrow$ LUMO+1 HOMO $\rightarrow$ LUMO+2 HOMO $\rightarrow$ LUMO+4 HOMO $\rightarrow$ LUMO+5	0.26594 0.11115 0.11023 0.16728 0.55847 -0.10637

Figure S25: Molecular orbitals involved in the most optically active electronic transitions of **2**.



## Results for 3

The geometry used for the simulation of the electronic absorption spectrum is the following:

Center Number	Atomic Number	Atomic Type	Coordinates (Angstroms)		
			X	Y	Z
1	6	0	0.298046	2.391217	0.972406
2	6	0	0.620126	2.077788	2.315669
3	6	0	0.467879	3.040133	3.329881
4	6	0	-0.005411	4.330915	3.014179
5	6	0	-0.329425	4.649490	1.681999
6	6	0	-0.182137	3.682649	0.666534
7	1	0	0.990015	1.072148	2.558560
8	1	0	0.720247	2.786069	4.368274
9	1	0	-0.122141	5.083560	3.805430
10	1	0	-0.701900	5.651876	1.430980
11	1	0	-0.444150	3.928874	-0.371054
12	6	0	0.452253	1.270626	-0.126649
13	6	0	1.916661	0.711864	-0.131569
14	6	0	2.161391	-0.675226	-0.150706
15	6	0	3.025575	1.590365	-0.161640
16	6	0	3.471593	-1.184062	-0.194864
17	1	0	1.304690	-1.362566	-0.131643
18	6	0	4.335619	1.096675	-0.202504
19	1	0	2.861211	2.676302	-0.138778
20	6	0	4.591680	-0.307669	-0.222837
21	1	0	3.614805	-2.268735	-0.219172
22	1	0	5.171768	1.804622	-0.203987
23	7	0	5.967628	-0.794454	-0.163865
24	6	0	6.943523	-0.098113	-1.088715
25	1	0	6.874838	0.992393	-0.935349
26	1	0	6.718655	-0.318100	-2.155377
27	6	0	8.403993	-0.567683	-0.756789
28	1	0	8.656880	-0.249285	0.280465
29	1	0	9.111731	-0.084013	-1.460360
30	6	0	6.146013	-2.289631	-0.263390
31	1	0	5.847645	-2.682143	-1.260172
32	1	0	5.519076	-2.772593	0.507451
33	6	0	7.648436	-2.651842	0.019903
34	1	0	7.785418	-3.746332	-0.094636
35	1	0	7.889783	-2.370141	1.070434
36	8	0	8.579990	-2.019544	-0.928567
37	8	0	-0.401277	0.112279	0.311042
38	6	0	0.084002	1.775635	-1.542205
39	1	0	0.885277	2.266943	-2.107844
40	6	0	-1.155422	1.605892	-2.043304
41	1	0	-1.403756	1.968315	-3.049023
42	6	0	-2.184418	0.881526	-1.267697
43	6	0	-1.744023	0.165501	-0.132917
44	6	0	-2.626162	-0.709031	0.592353
45	1	0	-2.194693	-1.304342	1.404028
46	6	0	-3.966292	-0.830410	0.233801
47	6	0	-4.493332	-0.014952	-0.863623
48	6	0	-3.588564	0.811017	-1.633632
49	6	0	-4.135184	1.571550	-2.728788
50	1	0	-3.464435	2.197027	-3.329742
51	6	0	-5.491191	1.543247	-3.023981
52	1	0	-5.883555	2.136912	-3.860648
53	6	0	-6.387819	0.770157	-2.225795
54	1	0	-7.463957	0.788174	-2.441965
55	6	0	-5.895865	0.013138	-1.170977
56	1	0	-6.576907	-0.556945	-0.527139
57	7	0	-4.931387	-1.673449	0.959297
58	6	0	-5.379847	-2.892446	0.177775
59	1	0	-6.293023	-3.277665	0.670909
60	1	0	-5.637832	-2.581216	-0.848109
61	6	0	-4.267891	-4.030739	0.135208
62	1	0	-4.733949	-5.007819	0.403400
63	1	0	-3.847665	-4.115344	-0.886607
64	8	0	-3.111944	-3.745527	1.004397
65	6	0	-3.642718	-3.442570	2.344391
66	1	0	-2.756830	-3.318489	2.998514
67	1	0	-4.248526	-4.290703	2.737605
68	6	0	-4.515603	-2.114123	2.345493
69	1	0	-5.447637	-2.292448	2.917321
70	1	0	-3.971849	-1.281988	2.823178

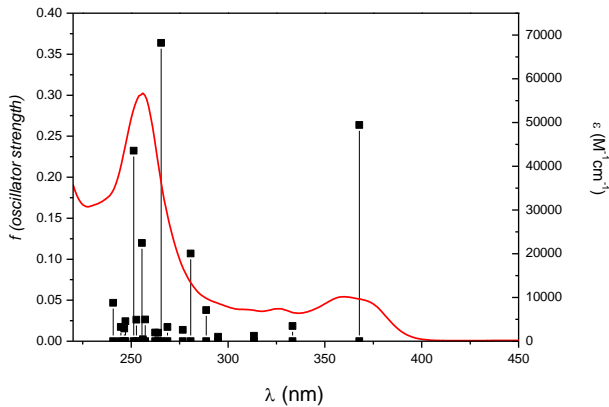
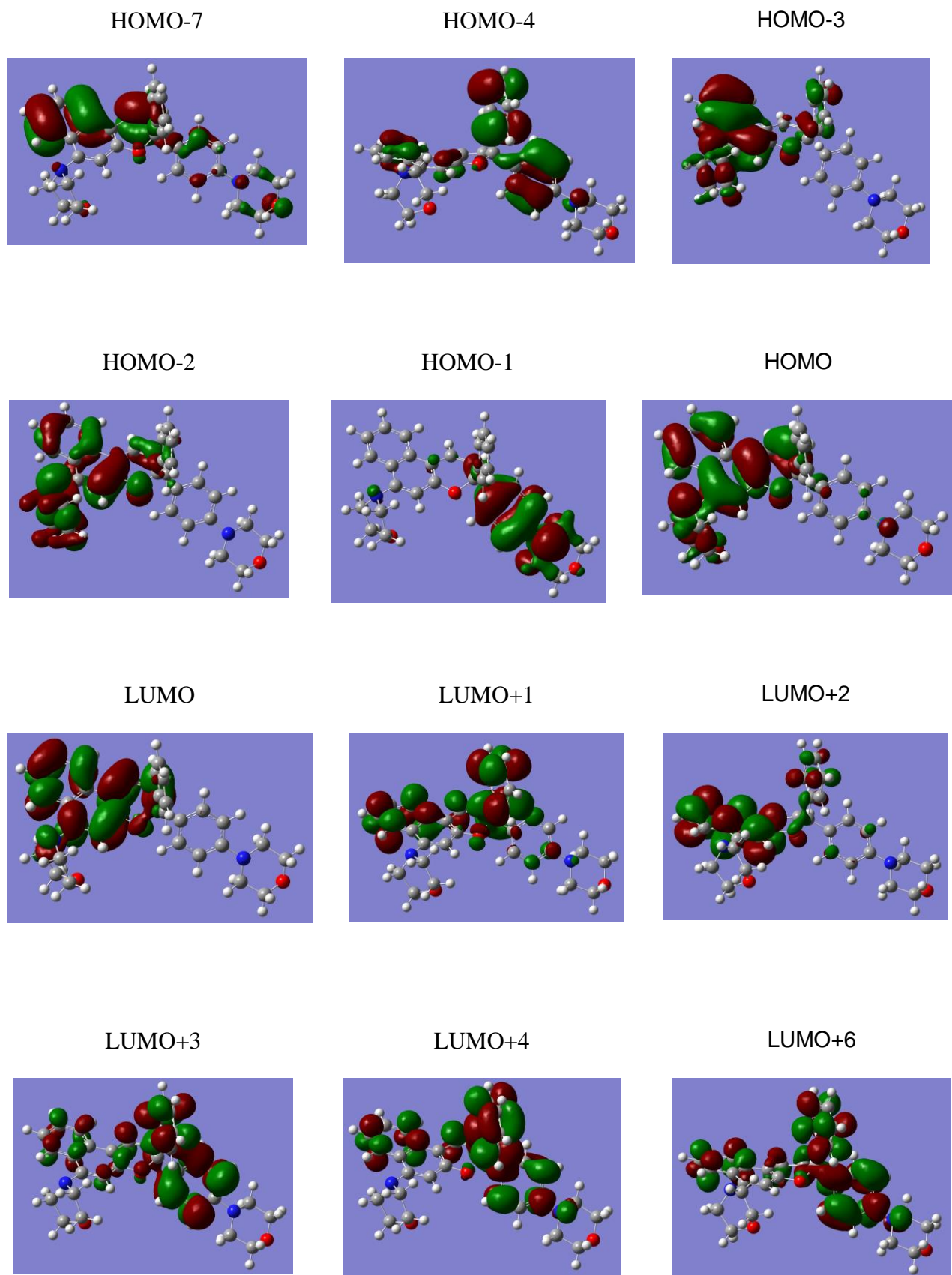


Figure S26: Electronic absorption spectrum of **3** (red trace) compared with the simulated oscillator strengths of the optically active transitions (vertical segments ending with a squared black dot).

Table S3: The principal optically active transitions of **3**, simulated by DFT 6-31G including the contribution of acetonitrile.

$\lambda$ (nm)	f(oscillator strength)	Orbitals	Weightings
367.74	0.2637	HOMO $\rightarrow$ LUMO	0.65120
280.75	0.1068	HOMO $\rightarrow$ LUMO+3	0.61832
		HOMO $\rightarrow$ LUMO+4	-0.26826
265.45	0.3637	HOMO-4 $\rightarrow$ LUMO	-0.26091
		HOMO-3 $\rightarrow$ LUMO	0.46446
		HOMO-2 $\rightarrow$ LUMO	0.11664
		HOMO-2 $\rightarrow$ LUMO+1	-0.10643
		HOMO-1 $\rightarrow$ LUMO+1	0.12300
		HOMO $\rightarrow$ LUMO+2	-0.24901
		HOMO $\rightarrow$ LUMO+3	0.10446
255.59	0.1198	HOMO-4 $\rightarrow$ LUMO	0.36065
		HOMO-3 $\rightarrow$ LUMO	0.10500
		HOMO-2 $\rightarrow$ LUMO+2	0.10103
		HOMO-1 $\rightarrow$ LUMO+2	0.42722
		HOMO-1 $\rightarrow$ LUMO+3	-0.16604
		HOMO-1 $\rightarrow$ LUMO+4	0.17245
		HOMO $\rightarrow$ LUMO+6	-0.22797
251.34	0.2322	HOMO-7 $\rightarrow$ LUMO	0.17699
		HOMO-1 $\rightarrow$ LUMO+1	0.17641
		HOMO-1 $\rightarrow$ LUMO+2	-0.16265
		HOMO-1 $\rightarrow$ LUMO+4	0.58881

Figure S27: Molecular orbitals involved in the most optically active electronic transitions of **3**.



## Results for 4

The geometry used for the simulation of the electronic absorption spectrum is the following:

Center Number	Atomic Number	Atomic Type	Coordinates (Angstroms)		
			X	Y	Z
1	6	0	-2.649162	-0.840589	0.946841
2	6	0	-2.869042	-0.012097	2.074356
3	6	0	-3.218460	-0.573601	3.315494
4	6	0	-3.356508	-1.971452	3.444909
5	6	0	-3.138079	-2.801337	2.329122
6	6	0	-2.782456	-2.238571	1.086358
7	1	0	-2.760798	1.076342	1.971066
8	1	0	-3.385713	0.077980	4.183798
9	1	0	-3.631400	-2.410424	4.413375
10	1	0	-3.240416	-3.890778	2.425222
11	1	0	-2.602312	-2.887154	0.218812
12	6	0	-2.232119	-0.168871	-0.417955
13	6	0	-3.330480	0.859681	-0.867274
14	6	0	-2.970101	2.165050	-1.265359
15	6	0	-4.690481	0.473089	-0.911178
16	6	0	-3.955344	3.076372	-1.694175
17	1	0	-1.911438	2.454363	-1.226799
18	6	0	-5.673040	1.382824	-1.343814
19	1	0	-4.979005	-0.539322	-0.597951
20	6	0	-5.308024	2.687032	-1.735647
21	1	0	-3.665169	4.091291	-1.998094
22	1	0	-6.726970	1.074809	-1.372796
23	8	0	-1.011853	0.663548	-0.142846
24	6	0	-1.997102	-1.203646	-1.543607
25	1	0	-2.875448	-1.501107	-2.129203
26	6	0	-0.765931	-1.698620	-1.780719
27	1	0	-0.606080	-2.435498	-2.578301
28	6	0	0.397271	-1.212492	-1.010122
29	6	0	0.211791	-0.043156	-0.241180
30	6	0	1.315456	0.624478	0.390927
31	1	0	1.102471	1.569201	0.900084
32	6	0	2.607694	0.101730	0.321765
33	6	0	2.816343	-1.194816	-0.337037
34	6	0	1.716214	-1.821058	-1.038323
35	6	0	1.964731	-3.072143	-1.708525
36	1	0	1.145973	-3.553639	-2.256425
37	6	0	3.206742	-3.689434	-1.652750
38	1	0	3.368031	-4.647406	-2.165306
39	6	0	4.267966	-3.104121	-0.899065
40	1	0	5.230992	-3.624667	-0.817275
41	6	0	4.071720	-1.887912	-0.257767
42	1	0	4.869150	-1.453446	0.356809
43	7	0	3.759857	0.723195	0.968780
44	6	0	4.874700	1.157485	0.035893
45	1	0	5.819775	1.162370	0.613846
46	1	0	4.961280	0.430673	-0.789262
47	6	0	4.626007	2.595845	-0.557128
48	1	0	5.495052	2.888923	-1.180562
49	1	0	3.717514	2.572157	-1.202198
50	8	0	4.512782	3.623303	0.494247
51	6	0	3.336981	3.255780	1.306008
52	1	0	2.405086	3.299531	0.698635
53	1	0	3.268600	4.017616	2.108964
54	6	0	3.489668	1.828700	1.960910
55	1	0	2.590180	1.573734	2.548668
56	1	0	4.358796	1.855901	2.647436
57	1	0	-6.076313	3.396466	-2.070953

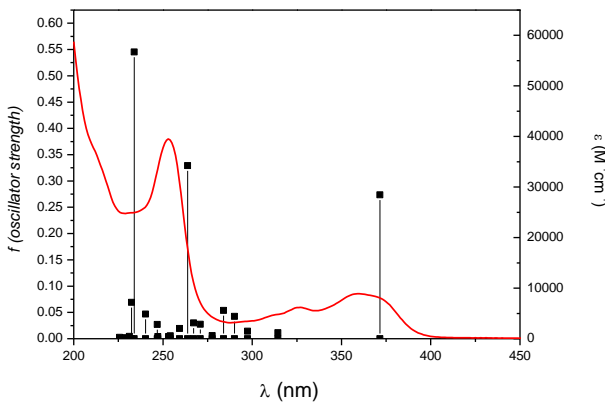
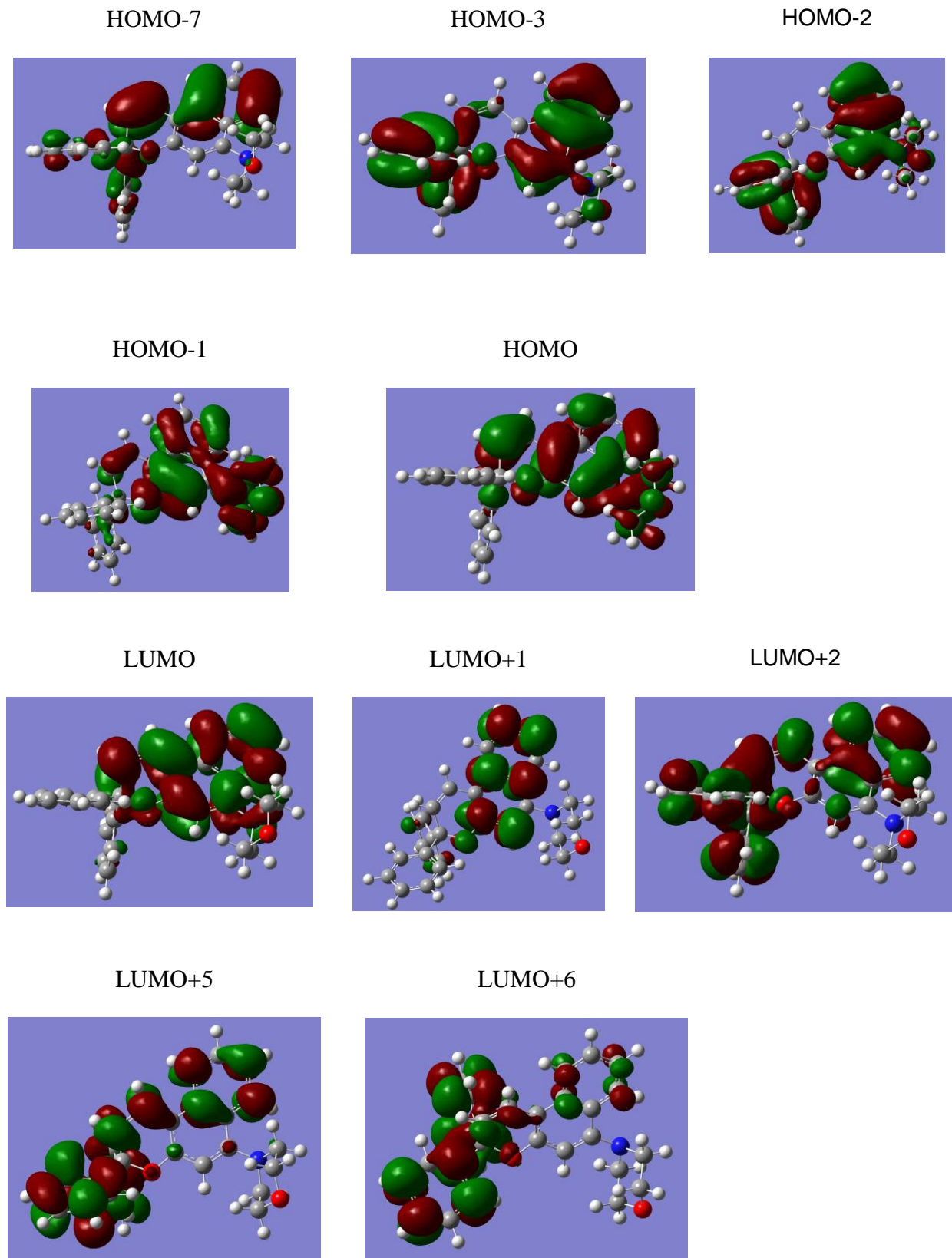


Figure S28: Electronic absorption spectrum of **4** (red trace) compared with the simulated oscillator strengths of the optically active transitions (vertical segments ending with a squared black dot).

Table S4: The principal optically active transitions of **4**, simulated by DFT 6-31G including the contribution of acetonitrile.

$\lambda$ (nm)	f(oscillator strength)	Orbitals	Weightings
371.58	0.2736	HOMO $\rightarrow$ LUMO	0.64941
263.81	0.3293	HOMO-7 $\rightarrow$ LUMO HOMO-3 $\rightarrow$ LUMO HOMO-2 $\rightarrow$ LUMO HOMO-1 $\rightarrow$ LUMO+1 HOMO $\rightarrow$ LUMO+1 HOMO $\rightarrow$ LUMO+5 HOMO $\rightarrow$ LUMO+6	-0.10216 0.42277 -0.22470 0.18678 0.24850 0.26039 -0.11901
233.87	0.5453	HOMO-7 $\rightarrow$ LUMO HOMO-1 $\rightarrow$ LUMO+1 HOMO-1 $\rightarrow$ LUMO+2 HOMO $\rightarrow$ LUMO+1	-0.21339 0.48160 -0.25781 -0.10134

Figure S29: Molecular orbitals involved in the most optically active electronic transitions of **4**.



## Results for 5

The geometry used for the simulation of the electronic absorption spectrum is the following:

Center Number	Atomic Number	Atomic Type	Coordinates (Angstroms)		
			X	Y	Z
1	6	0	7.027134	-1.953703	-0.639867
2	6	0	6.349984	-1.972504	0.570444
3	6	0	4.968939	-1.578407	0.652079
4	6	0	4.277976	-1.156995	-0.547983
5	6	0	5.017014	-1.150115	-1.785256
6	6	0	6.349378	-1.536787	-1.828467
7	1	0	4.784618	-1.933802	2.808235
8	1	0	8.081421	-2.255456	-0.693093
9	1	0	6.859150	-2.289553	1.490902
10	6	0	4.254233	-1.600786	1.905532
11	6	0	2.883523	-0.756940	-0.462961
12	1	0	4.517535	-0.826441	-2.706291
13	1	0	6.893636	-1.521487	-2.782442
14	6	0	2.242588	-0.757533	0.795553
15	6	0	2.932695	-1.206160	1.980714
16	1	0	2.382727	-1.218099	2.930884
17	8	0	0.883461	-0.427899	1.013139
18	6	0	2.046815	-0.416403	-1.636547
19	1	0	2.432984	-0.622562	-2.642636
20	6	0	0.809173	0.085371	-1.469018
21	1	0	0.146929	0.309221	-2.314053
22	6	0	0.245830	0.399079	-0.058227
23	6	0	0.480260	1.924289	0.305192
24	6	0	0.968021	2.282711	1.578047
25	6	0	0.205376	2.973150	-0.627327
26	6	0	1.195326	3.628617	1.927444
27	1	0	1.170252	1.476113	2.295636
28	6	0	0.435354	4.331085	-0.280422
29	6	0	0.932245	4.650971	0.995176
30	1	0	1.578179	3.877243	2.925570
31	1	0	0.217084	5.113987	-1.018366
32	1	0	1.110011	5.701720	1.261157
33	9	0	-0.304036	2.684967	-1.874721
34	6	0	-1.285026	0.057162	0.011154
35	6	0	-1.767354	-0.958889	0.862947
36	6	0	-2.208223	0.756978	-0.799777
37	6	0	-3.133226	-1.274338	0.911979
38	1	0	-1.053376	-1.502898	1.495716
39	6	0	-3.574901	0.452165	-0.768056
40	1	0	-1.829931	1.554105	-1.458961
41	6	0	-4.069137	-0.576834	0.090805
42	1	0	-3.483291	-2.057835	1.592243
43	1	0	-4.268306	1.008459	-1.407363
44	7	0	-5.464943	-0.862478	0.171252
45	6	0	-6.434152	-0.298638	-0.825301
46	1	0	-6.140662	-0.543252	-1.869715
47	1	0	-6.487810	0.803422	-0.730887
48	6	0	-7.781014	-0.986542	-0.448427
49	1	0	-8.472586	-1.033524	-1.304950
50	1	0	-8.268531	-0.429561	0.368532
51	6	0	-7.348687	-2.401898	0.044785
52	1	0	-8.077603	-2.841414	0.744238
53	1	0	-7.237282	-3.083489	-0.814544
54	6	0	-5.957640	-2.172510	0.725066
55	1	0	-5.251747	-2.995486	0.494293
56	1	0	-6.055198	-2.107152	1.828840

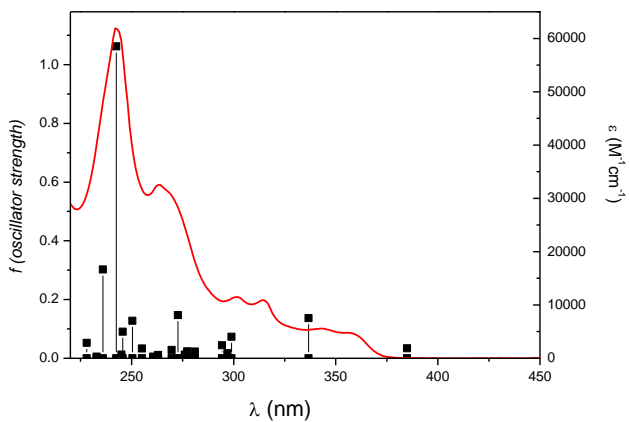
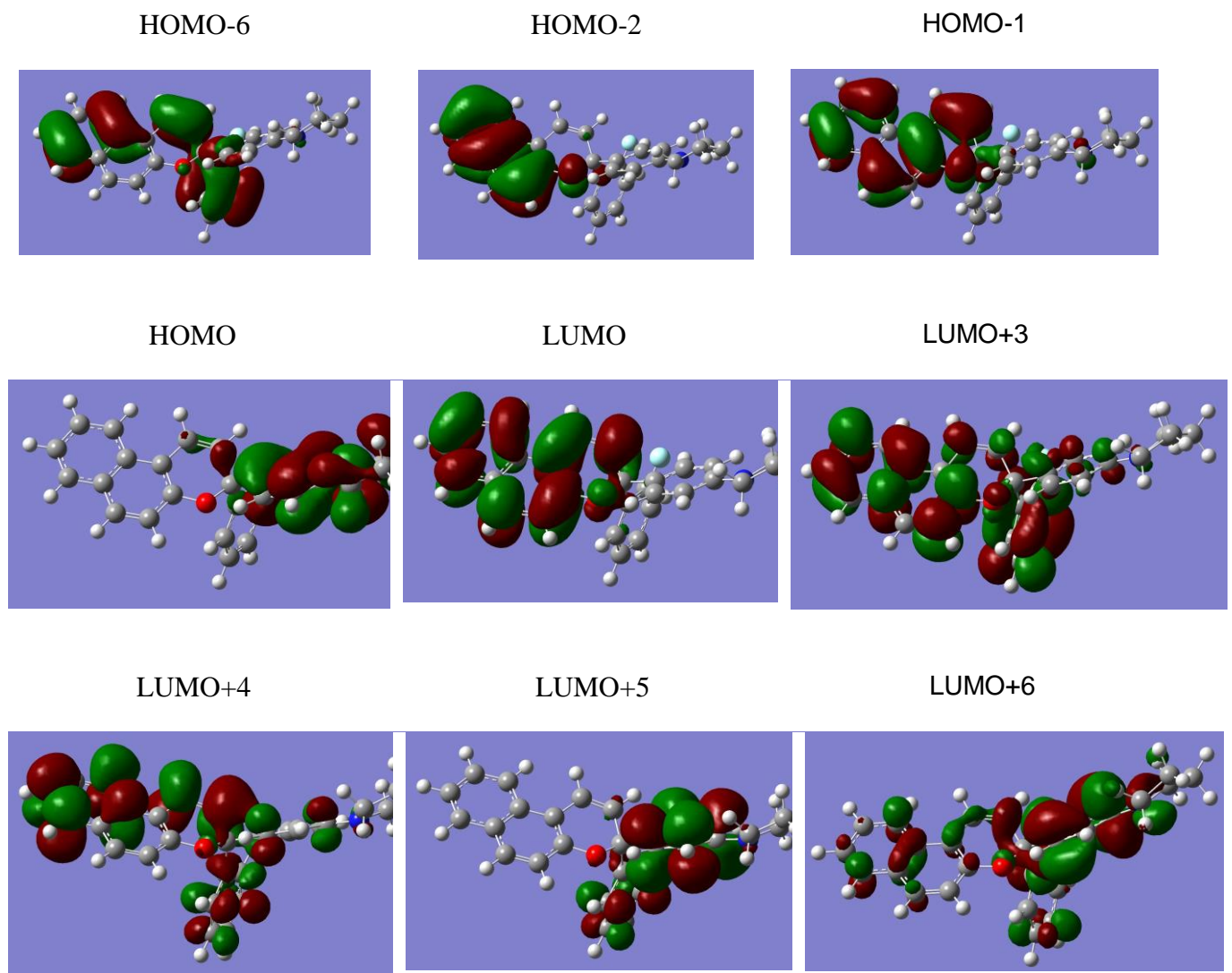


Figure S30: Electronic absorption spectrum of **5** (red trace) compared with the simulated oscillator strengths of the optically active transitions (vertical segments ending with a squared black dot).

Table S5: The principal optically active transitions of **5**, simulated by DFT 6-31G including the contribution of acetonitrile.

$\lambda$ (nm)	f(oscillator strength)	Orbitals	Weightings
336.67	0.1363	HOMO-1 ->LUMO	0.64115
272.67	0.1471	HOMO-1 ->LUMO+3 HOMO ->LUMO+4 HOMO ->LUMO+5	-0.11412 0.59690 0.29024
242.48	1.0620	HOMO-6 ->LUMO HOMO-2 ->LUMO HOMO-1 ->LUMO+3 HOMO-1 ->LUMO+4 HOMO-1 ->LUMO+5 HOMO ->LUMO+6	0.25487 0.11968 -0.13221 -0.15789 0.13177 0.52229

Figure S31: Molecular orbitals involved in the most optically active electronic transitions of **5**.



## References

S9. Gaussian 03, Revision C.02, M. J. Frisch, G. W. Trucks, H. B. Schlegel, G. E. Scuseria, M. A. Robb, J. R. Cheeseman, J. A. Montgomery, Jr., T. Vreven, K. N. Kudin, J. C. Burant, J. M. Millam, S. S. Iyengar, J. Tomasi, V. Barone, B. Mennucci, M. Cossi, G. Scalmani, N. Rega, G. A. Petersson, H. Nakatsuji, M. Hada, M. Ehara, K. Toyota, R. Fukuda, J. Hasegawa, M. Ishida, T. Nakajima, Y. Honda, O. Kitao, H. Nakai, M. Klene, X. Li, J. E. Knox, H. P. Hratchian, J. B. Cross, V. Bakken, C. Adamo, J. Jaramillo, R. Gomperts, R. E. Stratmann, O. Yazyev, A. J. Austin, R. Cammi, C. Pomelli, J. W. Ochterski, P. Y. Ayala, K. Morokuma, G. A. Voth, P. Salvador, J. J. Dannenberg, V. G. Zakrzewski, S. Dapprich, A. D. Daniels, M. C. Strain, O. Farkas, D. K. Malick, A. D. Rabuck, K. Raghavachari, J. B. Foresman, J. V. Ortiz, Q. Cui, A. G. Baboul, S. Clifford, J. Cioslowski, B. B. Stefanov, G. Liu, A. Liashenko, P. Piskorz, I. Komaromi, R. L. Martin, D. J. Fox, T. Keith, M. A. Al-Laham, C. Y. Peng, A. Nanayakkara, M. Challacombe, P. M. W. Gill, B. Johnson, W. Chen, M. W. Wong, C. Gonzalez, and J. A. Pople, Gaussian, Inc., Wallingford CT, 2004.

### Reflectance properties of paper impregnated with the best quaternary mixture after irradiation by UVA, UVB and UVC

Reflectance measurements were performed using a spectrophotometer composed of Avantes parts and a deuterium-halogen lamp (AvaLight-DH-2000-FHS). An integrating sphere with a 6 mm diameter viewing aperture and 8° irradiation angle (ISP-30-6) was used to collect and transfer reflectance signals to an AvaSpec-2048 charge-coupled device detector via a quartz fiber-optic system.

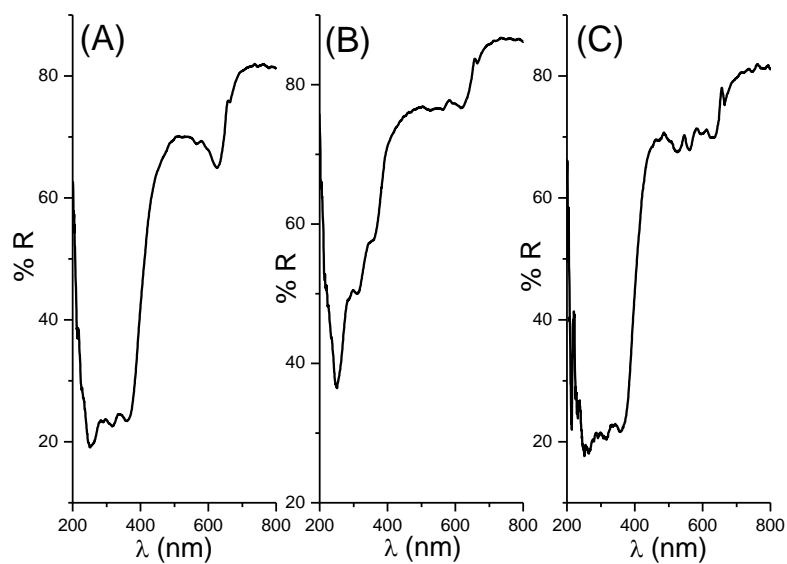


Figure S32: Reflectance spectra paper impregnated with best dye composition after irradiation with UVA (A), UVB (B) and UVC (C).